118

BioRadiations

A Resource for Life Science Research

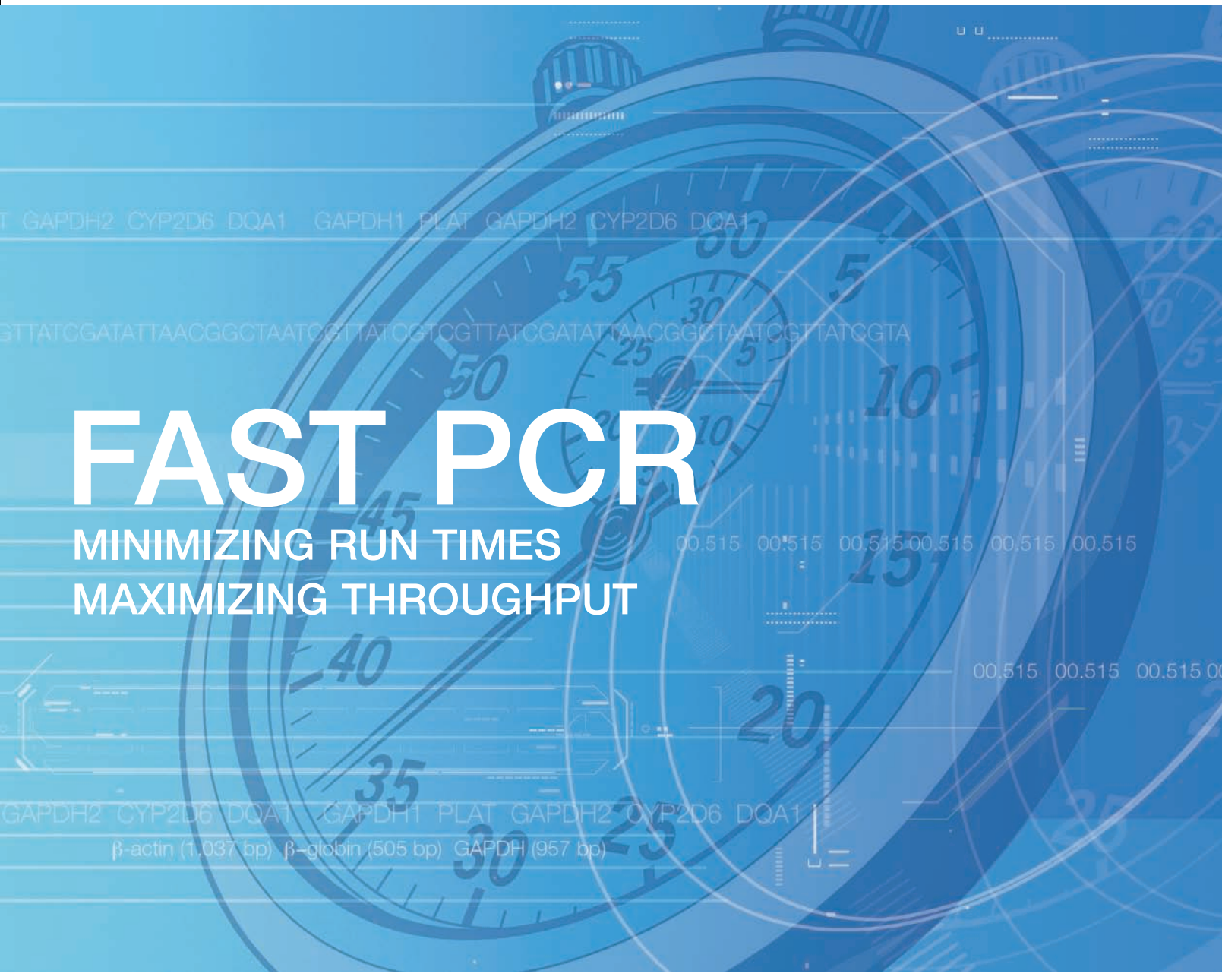

FAST PCR

MINIMIZING RUN TIMES
MAXIMIZING THROUGHPUT

In this issue:

BIO-RAD

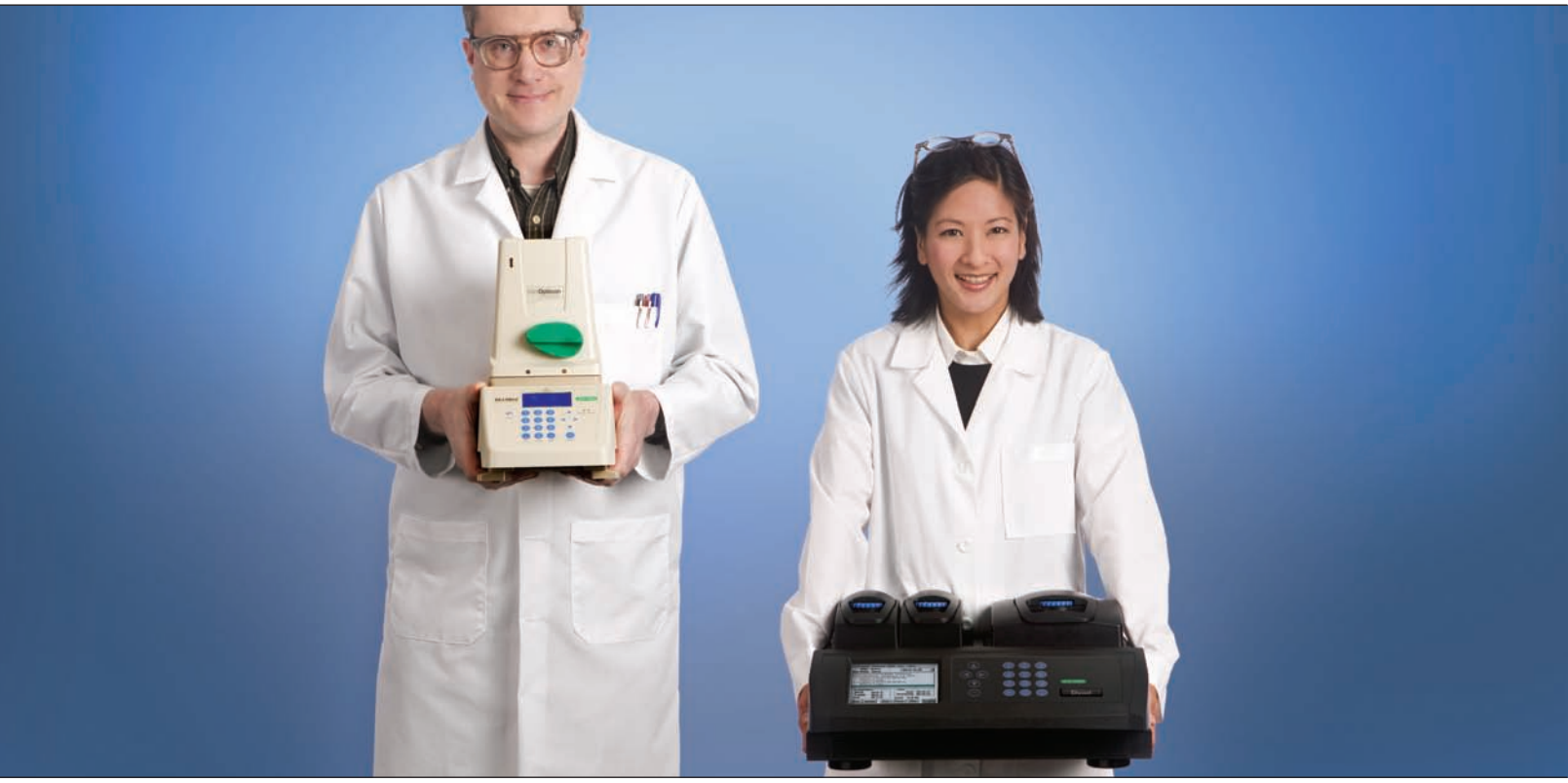

One just right for you.

Find your perfect match among the full line of Bio-Rad amplification products.

Bio-Rad is committed to providing you with the best tools for your PCR needs. This dedication is proven by our history of innovation, quality, and regard for researchers' needs.

- The most complete line of thermal cyclers available anywhere
- The only modular real-time cycler upgrade with a thermal gradient; choose from 1 to 5 colors
- Innovative enzymes that work where others fail
- PCR tubes, plates, and sealers for any application
- Dedicated technical support by experienced scientists

Back in the USA

Bio-Rad announces that the litigation surrounding its real-time systems and former MJ thermal cycler products has been resolved, and all products are available in the US.

Find out more at **www.bio-rad.com/PCRnews/**

For more information, visit us on the Web at **www.bio-rad.com/amplification/**

Photo: Pete with his MiniOpticon™ real-time system and Patty with her DNA Engine Dyad® cycler with a Dual Alpha™ unit and a single Alpha™ unit.

Visit us on the Web at **discover.bio-rad.com**
Call toll free at 1-800-4BIORAD (1-800-424-6723);
outside the US, contact your local sales office.

BIO-RAD

BIO-RAD SUBSIDIARY
TELEPHONE NUMBERS

Australia 61-2-9914-2800
Austria 43-1-877-89-01
Belgium 32-9-385-55-11
Brazil 55-21-3237-9400
Canada 905-712-2771
China 86-21-6426-0808
Czech Republic 420-241-430-532
Denmark 45-44-52-10-00
Finland 358-9-804-22-00
France 33-1-47-95-69-65
Germany 49-89-318-84-0
Hong Kong 852-2-789-3300
Hungary 36-1-455-8800
India 91-124-402-9300
Israel 03-963-6050
Italy 39-06-5295892
Japan 81-3-5811-6270
Korea 82-2-3473-4460
Latin America 00-1-305-894-5950
Mexico 55-5200-05-20
The Netherlands 31-318-540666
New Zealand 64-9-415-2280
Norway 47-23-38-41-30
Poland 48-22-331-99-99
Portugal 351-21-472-7700
Russia 7-095-721-14-04
Singapore 65-6415-3188
South Africa 27-861-246-723
Spain 34-91-590-5200
Sweden 46-8-555-12700
Switzerland 41-61-717-9555
Taiwan 88-62-2578-7189
Thailand 662-651-8311
United Kingdom 44-20-8328-2000
USA Toll free 1-800-4BIORAD
(1-800-424-6723)

discover.bio-rad.com

On the cover:
Conceptual illustration by
Chris Crutchfield

BioRadiations magazine is published by
Bio-Rad Laboratories, Inc.
2000 Alfred Nobel Drive
Hercules, CA 94547 USA

BioRadiations

issue 118, 2006

TO OUR READERS

The ability of the polymerase chain reaction to reliably amplify distinct nucleotide sequences has revolutionized modern life science. While high product yield and high specificity — "abundance and distinction" as Nobel Prize winner Kary B Mullis characterized his "eureka" invention of the technique — have traditionally been the crucial PCR objectives, the rise of powerful software algorithms and instrumentation has led many researchers to focus increasingly on speed. How rapidly can abundant and accurate PCR results be obtained, and is new, expensive instrumentation necessary to achieve them? In our cover story, Bio-Rad scientists demonstrate how to achieve successful fast PCR results using traditional PCR instrumentation coupled with intelligent experimental design.

COVER STORY

DEPARTMENTS

TECHNICAL REPORTS

PRODUCT FOCUS

Legal Notices

Experion™ Software Version 2.0

Experion software 2.0 adds significant features to Bio-Rad's easy-to-use automated electrophoresis software package.

Chip Compare Feature

- Compare samples across multiple chips for more powerful comparisons of various samples
- Share data with collaborators and combine your results into one screen for easy comparison of similarities and differences between samples

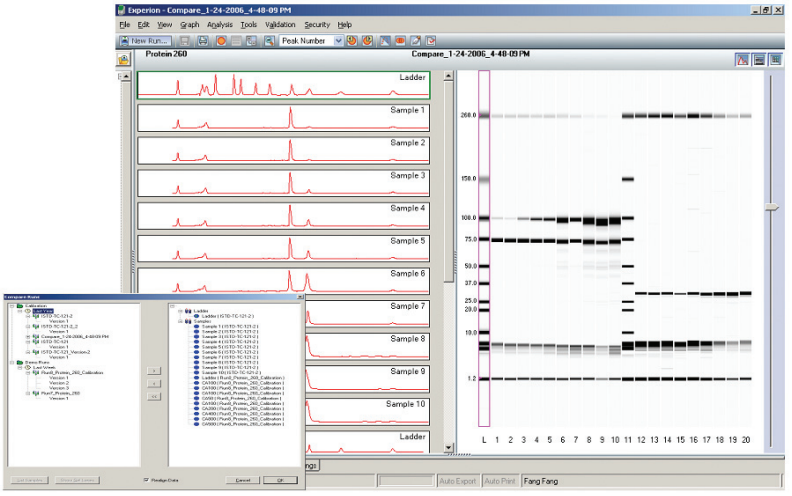

Chip compare feature.

Sample Quantitation Calculations

The software offers three ways to determine unknown protein concentration:

- Calculate relative concentration as compared to the Upper Marker (default)
- Create a calibration curve to calculate the concentration
- Achieve absolute quantitation by selecting your internal standards of choice

For regulatory labs, Experion software version 2.0 also supports two new optional packages, the validation kit and Security Edition software.

Experion Validation Kit (Optional)

The installation qualification and operational qualification (IQ/OQ) validation kit includes protocols that test critical instrument parameters to verify and validate specified functionality. Validation should be performed at least biannually, and also when troubleshooting or after moving the instrument. The kit allows you to:

- Ensure reliability and consistency of your analytical results
- Automate validation process with procedures built into the software
- Perform routine instrument maintenance and validation procedures

Experion Security Edition Software (Optional)

Automation makes the Experion system ideal for research in a regulated laboratory environment. The optional Security Edition offers tools for compliance with US FDA 21 CFR Part 11 regulations.

- Authorization system provides secure user log-in and allows the assignment of different levels for control of access to different functions
- Audit trail table provides security and control by tracking daily use of the system

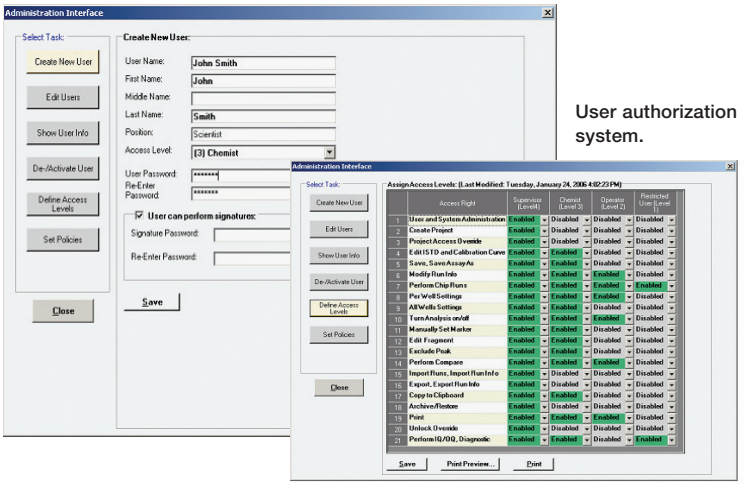

User authorization system.

- Database and file integrity ensured with password protection and auto-lock function
- Electronic signatures for easy record keeping and tracking
- Run version history conveniently presents information on various versions of a run in one easy-to-view dialog box
- Report generation allows quick viewing and archiving of multiple run parameters, data, audit trail, and electronic signatures

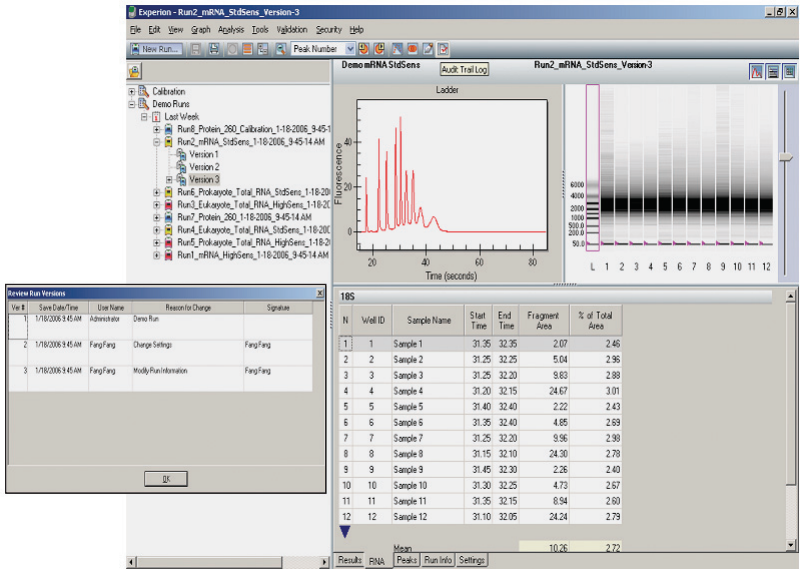

Run version history.

Quick Access to Information

- Automatic calculations to provide information for a variety of protein and RNA samples — size, concentration, percent of total sample, and ribosomal RNA ratio and ribosomal RNA contamination percentage in mRNA samples
- Multichip comparison function to easily identify similarities and differences among several samples from different runs
- User-defined internal standard option for absolute quantitation
- Query-based comparisons of a single peak across all samples in a chip to enable statistical analysis of expression of a single protein or RNA of interest
- Real-time display of data acquisition
- Multiple export capabilities for customized analysis, easy publication, and data sharing
- Overlay feature to allow direct comparison of multiple samples analyzed in different wells of chip

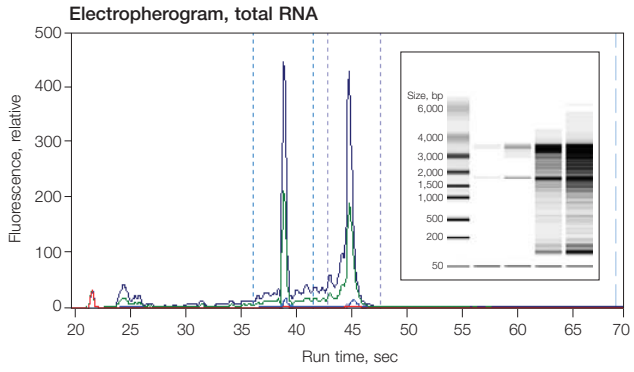

Overlay feature. Overlaying the individual electropherograms allows direct comparison of multiple RNA samples.

For more information, request bulletin 3171 or go to **www.bio-rad.com/experion/**

Ordering Information

Catalog #	Description
700-7050	Experion Software, system operation and standard data analysis tools, PC (comes with system orders, 700-7000, -7001, and -7002)
700-7051	Experion Validation Kit, 3 test chips, qualification procedures, dongle, PC
700-7052	Experion Security Edition Software, system operation and standard and 21 CFR 11 data analysis tools, 3 test chips, qualification procedures, dongle, PC

Bio-Plex™ Phosphoprotein and Total Target Assays

The Growing List of Signal Transduction Assays Now Includes NF-κB p65 and S6 Ribosomal Protein

The latest additions to the Bio-Plex phosphoprotein detection product line include phospho-c-Jun, phospho-HSP27, phospho-NF-κB p65, phospho-p53, phospho-p70 S6 kinase, phospho-p90RSK, phospho-S6 ribosomal protein, phospho-STAT2, phospho-TrkA, total Akt, total c-Jun, and total p90RSK. These easy-to-use bead-based multiplexable assays (based on xMAP technology) feature antibodies exclusively developed by Cell Signaling Technology, Inc. They are available individually or as x-Plex™ assays, which are specially premixed and quality-tested at Bio-Rad.

For more information, visit us on the Web at **www.bio-rad.com/products/phosphoproteins/**

Ordering Information

Catalog #	Description
Reagent Kits	
171-304004	Bio-Plex Phosphoprotein Detection Reagent Kit, 1 x 96-well
171-304005	Bio-Plex Phosphoprotein Detection Reagent Kit, 10 x 96-well
Sample Preparation Kits	
171-304011	Bio-Plex Cell Lysis Kit, 1 x 96-well
171-304012	Bio-Plex Cell Lysis Kit, 10 x 96-well
Phosphoprotein Assays	
171-V21075	Bio-Plex Phospho-Akt (Ser^{473}) Assay, 1 x 96-well
171-V21620*	Bio-Plex Phospho-ATF-2 (Thr^{71}) Assay, 1 x 96-well
171-V24356*	Bio-Plex Phospho-c-Jun (Ser^{63}) Assay, 1 x 96-well
171-V23120**	Bio-Plex Phospho-EGFR (Tyr) Assay, 1 x 96-well
171-V21938	Bio-Plex Phospho-ERK1 (Thr^{202}/Tyr^{204}) Assay, 1 x 96-well
171-V20438	Bio-Plex Phospho-ERK2 (Thr^{185}/Tyr^{187}) Assay, 1 x 96-well
171-V22238	Bio-Plex Phospho-ERK1/2 (Thr^{202}/Tyr^{204}, Thr^{185}/Tyr^{187}) Assay, 1 x 96-well
171-V23318	Bio-Plex Phospho-GSK-3α/β (Ser^{21}/Ser^{9}) Assay, 1 x 96-well
171-V24551	Bio-Plex Phospho-HSP27 (Ser^{78}) Assay, 1 x 96-well
171-V20758*	Bio-Plex Phospho-IκB-α (Ser^{32}/Ser^{36}) Assay, 1 x 96-well
171-V21034	Bio-Plex Phospho-JNK (Thr^{183}/Tyr^{185}) Assay, 1 x 96-well
171-V24937*	Bio-Plex Phospho-NF-κB p65 (Ser^{536}) Assay, 1 x 96-well
171-V21336	Bio-Plex Phospho-p38 MAPK (Thr^{180}/Tyr^{182}) Assay, 1 x 96-well
171-V25153	Bio-Plex Phospho-p53 (Ser^{15}) Assay, 1 x 96-well
171-V24155	Bio-Plex Phospho-p70 S6 Kinase (Thr^{421}/Ser^{424}) Assay, 1 x 96-well
171-V23535	Bio-Plex Phospho-p90RSK (Thr^{359}/Ser^{363}) Assay, 1 x 96-well
171-V25374**	Bio-Plex Phospho-S6 Ribosomal Protein (Ser^{235}/Ser^{236}) Assay, 1 x 96-well
171-V23732	Bio-Plex Phospho-STAT2 (Tyr^{689}) Assay, 1 x 96-well
171-V22552	Bio-Plex Phospho-STAT3 (Tyr^{705}) Assay, 1 x 96-well
171-V23973	Bio-Plex Phospho-TrkA (Tyr^{490}) Assay, 1 x 96-well
Total Target Assays	
171-V31075	Bio-Plex Total Akt Assay, 1 x 96-well
171-V31620*	Bio-Plex Total ATF-2 Assay, 1 x 96-well
171-V34356*	Bio-Plex Total c-Jun Assay, 1 x 96-well
171-V30438	Bio-Plex Total ERK2 Assay, 1 x 96-well
171-V30758	Bio-Plex Total IκB-α Assay, 1 x 96-well
171-V31034	Bio-Plex Total JNK Assay, 1 x 96-well
171-V31336	Bio-Plex Total p38 MAPK Assay, 1 x 96-well
171-V33535	Bio-Plex Total p90RSK Assay, 1 x 96-well

* ATF-2 and c-Jun assays cannot be multiplexed together.
IκB-α and NF-κB p65 assays cannot be multiplexed together.
** These assays cannot be multiplexed.

Available Assays

	Bead Regions	
Assays	**Phosphoprotein**	**Total**
Akt (Ser^{473})	75	75 new
ATF-2 (Thr^{71})	20	20
c-Jun (Ser^{63})	56 new	56 new
EGFR (Tyr)	20	
ERK1 (Thr^{202}/Tyr^{204})	38	
ERK2 (Thr^{185}/Tyr^{187})	38	38
ERK1/2 (Thr^{202}/Tyr^{204}, Thr^{185}/Tyr^{187})	38	
GSK-3α/β (Ser^{21}/Ser^{9})	18	
HSP27 (Ser^{78})	51 new	
IκB-α (Ser^{32}/Ser^{36})	58	58
JNK (Thr^{183}/Tyr^{185})	34	34
NF-κB p65 (Ser^{536})	37 new	
p38 MAPK (Thr^{180}/Tyr^{182})	36	36
p53 (Ser^{15})	53 new	
p70 S6 kinase (Thr^{421}/Ser^{424})	55 new	
p90RSK (Thr^{359}/Ser^{363})	35 new	35 new
S6 ribosomal protein (Ser^{235}/Ser^{236})	74 new	
STAT2 (Tyr^{689})	32 new	
STAT3 (Tyr^{705})	52	
TrkA (Tyr^{490})	73 new	

Bio-Plex™ SNP Manager™ Macro

The Bio-Plex SNP Manager macro facilitates single nucleotide polymorphism (SNP) analysis and genotyping for nucleic acid applications using the Bio-Plex suspension array system. Obtain Bio-Plex SNP Manager at no cost from the Bio-Rad web site.

- Automatic allelic ratio calculation and gene calls are based on user-configured tolerance ranges
- User-configured error thresholds are used to flag abnormal results
- All data can be sorted, filtered, and graphed into histograms and scatter plots for easy analysis
- Graphs can be exported for use in reports and presentations
- Assay templates can be saved for reuse without additional configuration
- Automatic data import is easy directly from Bio-Plex Manager™ software into SNP Manager

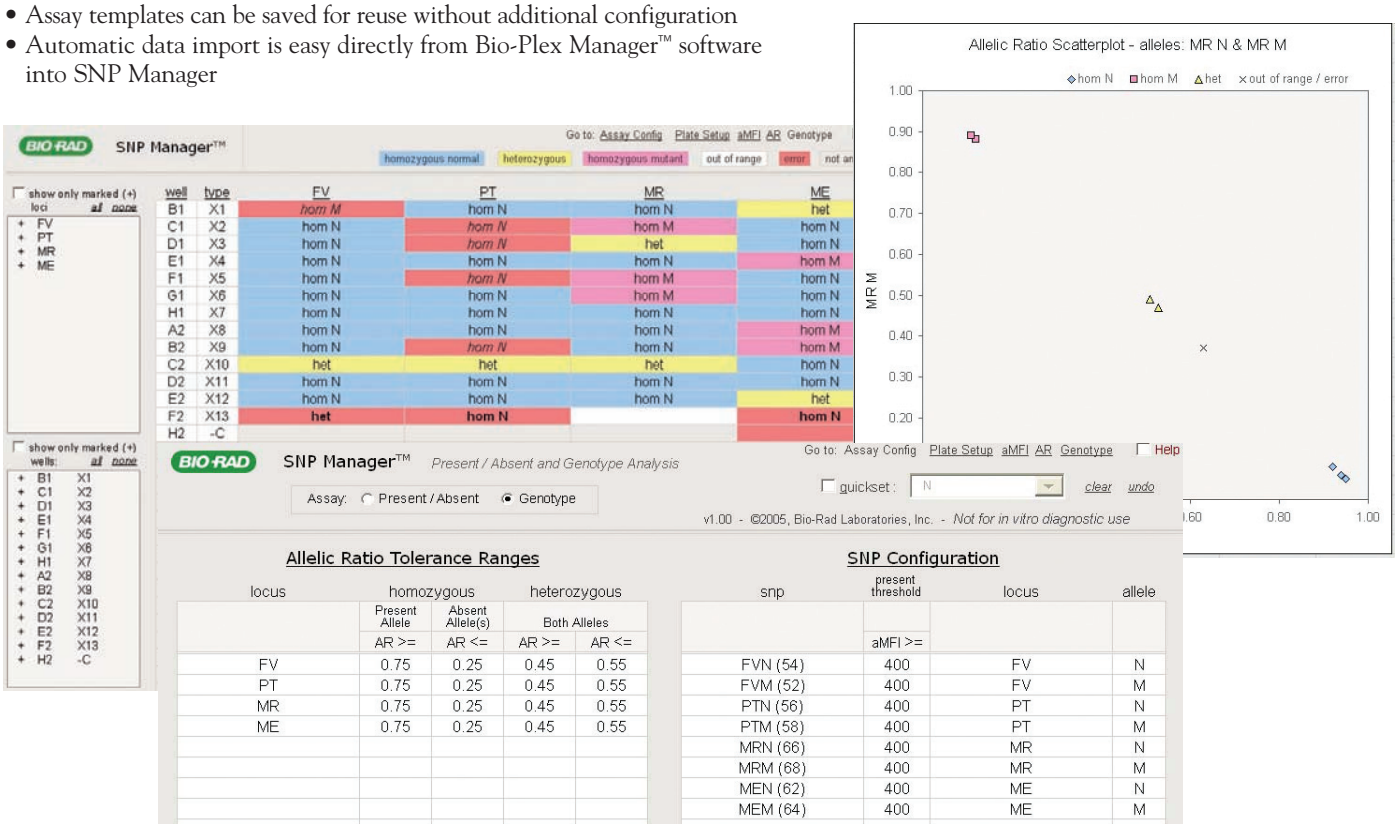

well	type	FV	PT	MR	ME
B1	X1	hom M	hom N	hom N	het
C1	X2	hom N	hom N	hom M	hom N
D1	X3	hom N	hom N	het	hom N
E1	X4	hom N	hom N	hom N	hom M
F1	X5	hom N	hom N	hom M	hom N
G1	X6	hom N	hom N	hom M	hom N
H1	X7	hom N	hom N	hom N	hom N
A2	X8	hom N	hom N	hom N	hom M
B2	X9	hom N	hom N	hom N	hom M
C2	X10	het	het	het	hom N
D2	X11	hom N	hom N	hom N	hom N
E2	X12	hom N	hom N	hom N	het
F2	X13	het	hom N		hom N
H2	-C				

locus	homozygous		heterozygous	
	Present Allele	Absent Allele(s)	Both Alleles	
	AR >=	AR <=	AR >=	AR <=
FV	0.75	0.25	0.45	0.55
PT	0.75	0.25	0.45	0.55
MR	0.75	0.25	0.45	0.55
ME	0.75	0.25	0.45	0.55

snp	present threshold	locus	allele
	aMFI >=		
FVN (54)	400	FV	N
FVM (52)	400	FV	M
PTN (56)	400	PT	N
PTM (58)	400	PT	M
MRN (66)	400	MR	N
MRM (68)	400	MR	M
MEN (62)	400	ME	N
MEM (64)	400	ME	M

For more information or to download the SNP Manager macro, go to **www.bio-rad.com/snpmanager/**

Flamingo™ Fluorescent Gel Stain

Flamingo fluorescent gel stain is a 10x solution containing a novel dye that fluoresces when bound to denatured proteins. This easy-to-use gel stain is appropriate for both 1-D and 2-D electrophoretic applications. The staining procedure is a simple two-step protocol that can be completed quickly. The steps are not time sensitive and destaining is not required. Stained gels may be stored in the dark at 2–8°C for up to 6 months without significant loss of imaging sensitivity.

Flamingo fluorescent gel stain is compatible with enzymatic digestion and mass spectrometry. Gels stained with Flamingo fluorescent gel stain can be imaged with a variety of imagers. The most optimal imaging systems are laser-based fluorescence scanners such as the Molecular Imager® PharosFX™ system. Other benefits include:

- Detection sensitivity of 0.5 ng and below
- Wide range of linearity (0.5 ng–1 µg)
- Low background
- Economical staining

High Sensitivity

Flamingo fluorescent gel stain will stain most proteins. The dye in the stain fluoresces only when bound to denatured proteins, and exhibits less protein-to-protein variability, making results more consistent and reproducible than with other staining methods.

Excellent Linearity

A broad linear range means that improved protein identification and quantitation can be achieved with fewer gels. Most gel stains are nonlinear at higher concentrations, leading to an increased chance of error. Flamingo fluorescent gel stain has excellent linearity over a broad range — 3 orders of magnitude — maximizing protein information obtained with each gel.

Low Background

Background makes it difficult to discriminate between speckles and spots. Gels stained with Flamingo fluorescent gel stain have less background, making results easier to see. Clearer results mean less guesswork.

Economy of Use

Flamingo is sold in a 10x solution, offering maximum product in minimal packaging. Flamingo costs less per gel than similar gel stains.

For more information, visit us on the Web at **www.bio-rad.com/flamingo/**

Ordering Information

Catalog #	Description
161-0490	Flamingo Fluorescent Gel Stain, 10x solution, 20 ml
161-0491	Flamingo Fluorescent Gel Stain, 10x solution, 100 ml
161-0492	Flamingo Fluorescent Gel Stain, 10x solution, 500 ml

Flamingo

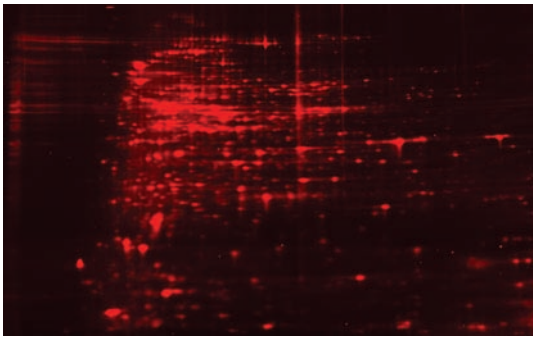

SYPRO Ruby

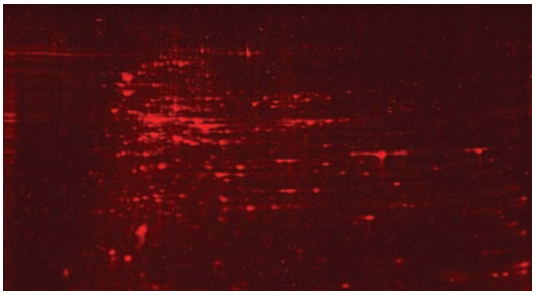

Comparison of 2-D gel staining with Flamingo vs. SYPRO Ruby. Total *E. coli* protein samples (10 µg) were separated by 2-D electrophoresis. Gels were stained with each dye according to manufacturer's instructions.

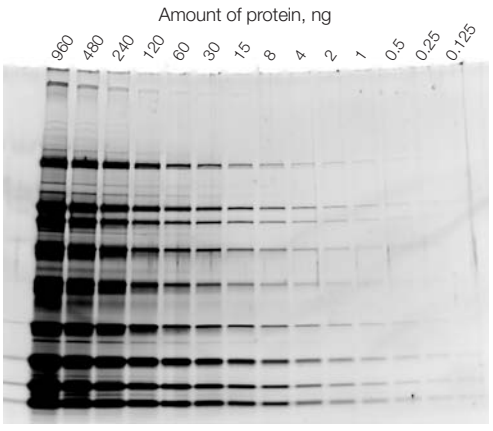

Excellent sensitivity using Flamingo fluorescent gel stain. A dilution series of Bio-Rad SDS-PAGE standards was run on a 4–20% Criterion™ Tris-HCl gel stained with Flamingo.

Improved Sealing Performance for Real-Time PCR

Due to the quantitative nature and inherent sensitivity of real-time PCR, it is important to minimize all sources of variability. One potential source is the method used for sealing reaction plates. An improperly applied film seal could lead to vapor loss from some wells, which could in turn lead to inaccurate data.

Microseal® 'B' clear seals are now validated and recommended for use in all Bio-Rad real-time PCR systems. These seals provide comparable light transmission to optical sealing tape, but they offer improved overall sealing performance and can be applied more reliably. These benefits are attributable to the thicker and more aggressive adhesive associated with Microseal 'B' seals.

The chart demonstrates that average reaction volume loss during two common real-time PCR protocols was significantly lower in reactions sealed with Microseal 'B' seals than in those sealed with optical sealing tape.

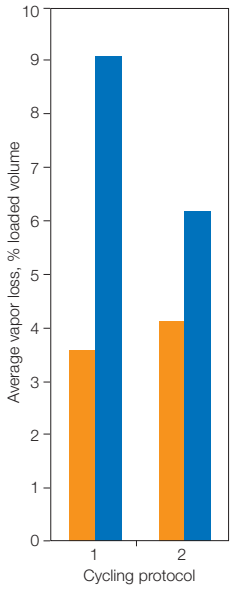

Improved sealing with Microseal 'B' seals. A 20 µl aliquot of test solution was added to every well of an iQ™ 96-well semi-skirted plate, sealed with either a Microseal 'B' seal (■ MSB-1001) or optical sealing tape (■ 223-9444), and then thermally cycled in an iCycler iQ® real-time PCR system using two different protocols. Protocol 1, probe-based qPCR: 95°C, 3 min; then 40 cycles of 95°C, 10 sec, and 55°C, 1 min. Protocol 2, SYBR Green qPCR plus melt curve: 95°C, 3 min; then 35 cycles of 94°C, 10 sec; 58°C, 30 sec; 72°C, 60 sec; then 72°C, 5 min; then a melt curve (increase 0.5°C from 72°C to 92.5°C every cycle, 8 sec/cycle). None of the sealing tests showed evidence of low or empty wells, but vapor retention was significantly improved with Microseal 'B' seals.

Amplification

- Amplification flier (bulletin 5386; PDF only)
- Consumables brochure (bulletin 5258)
- Improving reliability and reproducibility of real-time PCR reactions sealed with clear films (bulletin 5266; PDF only)
- iQ™ multiplex powermix flier (bulletin 5348)
- Long inverse PCR using iProof™ polymerase (bulletin 5337)
- Fast PCR flier (bulletin 5366)
- Reagents for reverse transcription, PCR, and real-time PCR brochure (bulletin 5345)
- Real-time PCR amplification instruments brochure (bulletin 5341)
- Thermal cyclers brochure (bulletin 5277)

Electrophoresis

- Flamingo™ fluorescent gel stain product information sheet (bulletin 5346)
- Fractionation by liquid-phase isoelectric focusing in the MicroRotofor™ cell: improved detection of low-abundance proteins (bulletin 5344)
- Monitoring the expression, purification, and processing of GST-tagged proteins using the Experion™ automated electrophoresis system (bulletin 3176)
- Protein expression, purification, and analysis brochure (bulletin 5304)
- Rapid and accurate protein sizing, quantitation, and analysis using the Experion automated system and the Experion Pro260 analysis kit product information sheet (bulletin 5351; PDF only)
- Using the Experion automated electrophoresis system to assess RNA quality and quantity in siRNA-induced gene silencing experiments (bulletin 5315)

Gene Transfer

- Gene expression brochure (bulletin 5303)
- Transfection of Caco-2 cells with siRNA using the siLentFect™ lipid reagent (bulletin 5370)

Imaging

- Molecular Imager® PharosFX™ system brochure (bulletin 5331)

Microarray Products

- BioOdyssey™ Calligrapher™ system brochure (bulletin 5338)
- BioOdyssey Calligrapher system flier (bulletin 5288)
- Demonstration of superior printing accuracy by the BioOdyssey Calligrapher miniarrayer (bulletin 5309)
- Reducing carryover contamination during microarray printing (bulletin 5310)
- Cooling characteristics of the BioOdyssey Calligrapher cooling module (bulletin 5403)

Multiplex Suspension Array Technology

- Bio-Plex™ assays product information sheet (bulletin 5325)
- Bio-Plex mouse cytokine assays (bulletin 3156)
- Simultaneous detection of multiple phosphoprotein targets from human tumor tissues using the Bio-Plex suspension array system (bulletin 5296)
- Use of the Bio-Plex cytokine immunoassay to determine cytokine expression levels in the intestinal mucosa (bulletin 5374)
- Feasibility of multiplexing Bio-Plex total target and phosphoprotein assays (bulletin 5312)

Sample Preparation

- Aurum™ total RNA fatty and fibrous tissue kit protocol overview (bulletin 5257)

Cooling Characteristics of the BioOdyssey™ Calligrapher™ Cooling Module

Theresa Redila-Flores, Cathleen Karlak, and Luis Ugozzoli, Bio-Rad Laboratories, Inc., Hercules, CA 94547 USA

Introduction

The BioOdyssey Calligrapher miniarrayer is a benchtop instrument for creating microarrays on various substrates. This instrument is capable of printing most soluble samples; however, temperature-sensitive molecules, such as proteins, require use of the optional cooling module, which allows cooling of both the source plate region and the platen to 10–15°C. When teamed with the humidity control module (HCM), the cooling module allows printing in a cooled environment while eliminating condensation at the slide surface. Here, we describe the efficiency of the cooling module at the various room temperatures and levels of humidity that may be encountered in laboratories worldwide.

Methods

The BioOdyssey Calligrapher system was used with the optional cooling system, which includes the HCM. For each run, fresh desiccant was placed in the HCM, the chiller was filled with 50% (v/v) ethylene glycol in water, and the temperature was adjusted to 0.0°C. The platen was cleared of all printing material, and two thermocouples were securely taped, one at the area labeled "Slide 1" and the other in the source plate region. Thermocouples were used to measure the actual temperatures of the platen and source plate region. The temperature of each of the thermocouples, the temperature of the chiller, and the humidity levels were recorded every 15 min for 90 min.

Results

To quantitate the cooling efficiency of the BioOdyssey Calligrapher miniarrayer cooling module, the platen, source plate, and chiller temperatures were first monitored at a constant humidity of 40%. When the initial platen temperature was set to 24°C (a typical room temperature), the platen and source plate region were cooled below 15°C within 60 min (Figure 1A); an additional 15–30 min period was required when the initial platen temperature was set to 32°C (Figure 1B).

Next, we tested whether humidity is a factor in temperature reduction. At an initial temperature of 24°C, we monitored the temperature reduction of the platen, source plate, and chiller at 40, 50, or 60% humidity (Figure 2). At all settings, 60 min was required for adequate cooling, which validates the results shown in Figure 1A and demonstrates that humidity does not appreciably affect temperature reduction.

Finally, we examined the correlation between the temperature displayed by the humidity control window in the graphical user interface (GUI) of the BioOdyssey Calligrapher miniarrayer (Figure 3) and the temperature data collected using the thermocouples. These values showed a linear correlation (Figure 4).

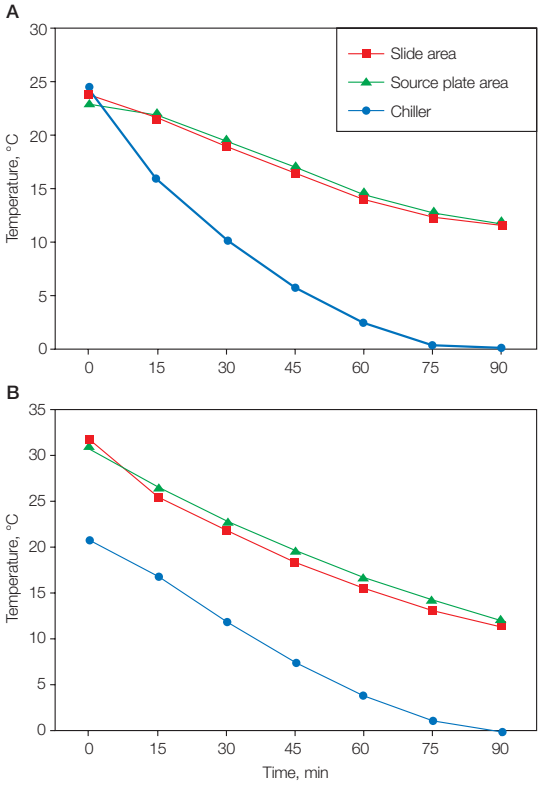

Fig. 1. Time course of slide and source plate temperature reduction. A, reduction from 24°C to 10°C; **B**, reduction from 32°C to 10°C. Humidity was set to 40%; values shown are averages obtained from three replicate experiments.

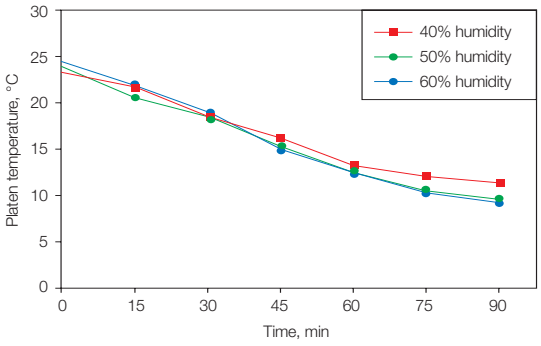

Fig. 2. Time course of slide and source plate temperature reduction at various humidity settings. Initial platen temperature was 24°C, and constant humidity was maintained with the HCM. Values shown are averages obtained from three replicate experiments.

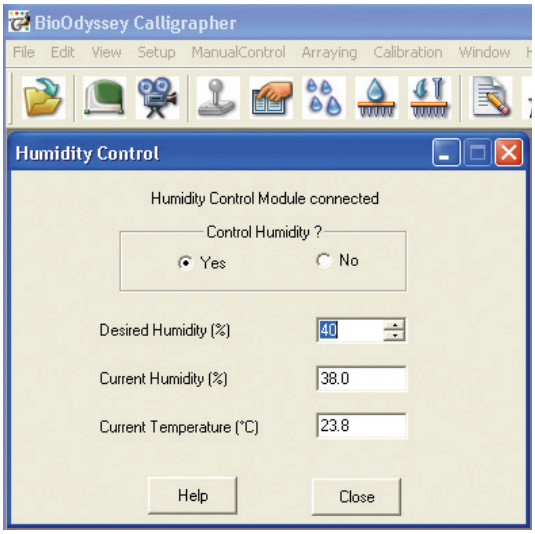

Fig. 3. Humidity control window.

Discussion

Many laboratories do not have optimal environmental temperature settings for printing microarrays. To allow effective use of the BioOdyssey Calligrapher miniarrayer's cooling module in different environments, we established a higher ambient temperature to understand the time required to effectively cool the unit. At a typical room temperature (24°C), the platen and the source plate were cooled to 10–15°C within 60 min; at the higher temperature of 32°C, an extra 15–30 min was required. In addition, we demonstrated that humidity plays a minimal role in temperature reduction, and based on our results, we recommend a humidity setting of 50%.

A common problem during cooling in many slide printing systems is the buildup of condensation on the slide surface. Condensation results in poor print runs, because the liquid causes the spots to merge. While performing this study, we monitored the platen for condensation, and, regardless of the humidity settings, none was observed. It is also important to point out that prior to each run fresh desiccant was added to ensure adequate dehumidification of the unit.

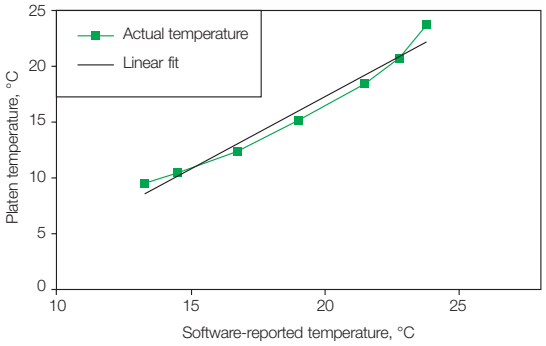

Fig. 4. Correlation between platen temperature as measured by the thermocouples and the chamber temperature as displayed by the GUI. Temperatures were measured at 50% humidity. Values shown are averages obtained from three replicate experiments. The equation of the best-fit line between the points was $y = 1.29x - 8.6322$, with an R^2 value of 0.972.

The temperature that is shown in the GUI is that of the Calligrapher's chamber, which is not identical to the platen temperature due to the positioning of the internal sensor. We have generated a formula (see Figure 4) that allows a more accurate indication of the actual platen temperature.

For additional copies of this article, request bulletin 5403.

Fluorescent Nanoparticles for Western Blotting

Kevin McDonald, Ahmed Elbaggari, and Marina Pekelis, Bio-Rad Laboratories, Inc., Hercules, CA 94547 USA

Introduction

Western blotting (Towbin et al. 1979, Renart et al. 1979) is a powerful method for identifying and analyzing protein targets. Many immunological detection systems have been developed to identify specific proteins blotted onto membranes, including autoradiographic, colorimetric, chemiluminescent, bioluminescent, chemifluorescent, fluorescent, and immunogold detection systems. These methods differ in their speed, sensitivity, and compatibility with multiplexing and quantitation.

Chemiluminescence is the predominant detection method for western blots, due to its speed and sensitivity compared to other methods (Kurien and Scofield 2003). Detection of protein in low picogram amounts is typical for chemiluminescence systems; these are more sensitive than most colorimetric systems, and approximately equal in sensitivity to radioisotopic detection. The biggest disadvantage of chemiluminescence detection is its incompatibility with multiplexing.

Another common method for identifying blotted proteins is fluorescence detection. Fluorescence detection can provide a 10-fold greater liner dynamic range than chemiluminescent methods, therefore providing better quantitation within the detection limits. Fluorescence detection also allows multiplex experiments to detect multiple antigens in a single probing step. Unfortunately, the sensitivity of most fluorescent blotting techniques is 2–4 times lower than that of analogous luminescence methods (Bio-Rad bulletin 2895).

Use of fluorescent semiconductor nanocrystals, or quantum dots (QDs), can overcome many of the handicaps of fluorescence detection, because QDs have unique optical properties that make them highly sensitive and well suited for optical multiplexing. First, unlike organic fluorophores, which absorb light of a particular wavelength, QDs absorb all wavelengths of light shorter than their emission wavelength. Therefore, a single light source emitting blue or shorter wavelengths can excite all QDs in a multiplex experiment, thereby significantly decreasing the cost and complexity of the setup. Second, the emission spectra of QDs, averaging 30 nm wide, are much more symmetrical than those of organic fluorophores. This affects both sensitivity and the ability to detect multiple targets in one imaging session. Because the emission spectra of organic fluorophores typically have extra peaks and long red tails, there can be considerable cross talk between channels. This cross talk decreases signal-to-noise ratio, and thus sensitivity. In contrast, the overlap between spectra of QDs is significantly less than for organic fluorophores (Alivisatos 1996). Furthermore, since the emission from QDs is concentrated in a narrow band, detection can be accomplished with narrow bandpass filters, which reject more background noise and auto-fluorescent contamination, increasing the sensitivity of detection. Finally, QDs are more photostable than organic fluorophores. This means that QD-labeled samples can be irradiated for long periods to improve sensitivity for better quantitation and reliability (Chan and Nie 1998, Wu et al. 2003).

In this article, we demonstrate the sensitivity and multiplex application of commercially available QD conjugates (Qdot conjugates from Invitrogen Corp.; originally developed by Quantum Dot Corp.) with various excitation and detection techniques, taking advantage of the flexibility of emission filter configuration allowed by Molecular Imager® VersaDoc™ and PharosFX™ systems. We also compare the detection limits of Qdot fluorescence and horseradish peroxidase (HRP) conjugate-based chemiluminescence.

Methods

Detection of Qdot QDs With Filters

Broad range biotinylated molecular weight standards (Bio-Rad catalog #161-0319) were separated on a Criterion™ 8–16% linear gradient gel, then transferred to an Immobilon-FL transfer membrane (Millipore Corp.). The blot was blocked with TBST buffer (Tris-buffered saline (TBS, 170-6435) containing 0.05% Tween 20 (161-0781)) and 3% dry milk (170-6404), then cut into vertical strips for detection with seven different streptavidin Qdot conjugates (Invitrogen #Q10151MP). Qdot QDs were diluted 1:1,000 in blocking solution. Fluorescence was detected on a PharosFX imager with 488 nm laser excitation and a VersaDoc 4000 imager with epi-UV excitation. The strips were imaged twice using different filters: those included with the instruments, and the Qdot-specific filters from Omega Optical Inc., recommended by Invitrogen.

On the PharosFX imager, Qdot-specific filters were inserted into blank filter cubes and added to the acquisition software according to the PharosFX instructions. The Qdot-specific filter was inserted in place of the clear glass in position 4 of the VersaDoc filter wheel and secured with a 25 mm diameter friction ring inserted on top of the filter. The 660SP filter was removed from the lens. In Quantity One® image acquisition software, a custom application was defined using filter position 4 for imaging the sample.

Comparison of Qdot Fluorescence and HRP-Based Chemiluminescence

To compare the detection limits of Q655 Qdot (Invitrogen) and Immun-Star™ HRP substrate, human transferrin (Sigma-Aldrich, Sweden) was detected using the dot-blot method. A series of 2-fold transferrin dilutions, beginning at 200 ng/ml, were made in 100 µg/ml BSA in TBS. A BSA solution was used as a control. A 50 µl aliquot of each dilution was loaded onto a Bio-Dot® microfiltration unit. The apparatus and protein solutions were left at room temperature (RT) for 2 hr before the solutions were drawn through the nitrocellulose membrane (162-0145) by applying a vacuum to the apparatus for about 10 min. The wells were washed twice with 200 µl TBS, which was drawn through the membrane in the same manner. The membrane was removed from the apparatus, cut in half, and blocked with Qdot blocker solution (Invitrogen) overnight at 4°C. After blocking, the membrane was incubated at RT for 1 hr with 1:6,000 rabbit anti-human transferrin antibody (Dako A/S, Denmark) in Qdot blocker. After 5 x 5 min washes in TBST, the two membrane pieces were placed in separate trays and incubated for 1 hr at RT with either 1:1,000 Qdot 655-conjugated goat anti-rabbit antibody (Invitrogen #Q11421MP) in Qdot blocker or with 1:15,000 HRP-conjugated goat anti-rabbit antibody (170-5046). The membranes were washed as before, then the Qdot 655 blot was placed in TBS while the HRP blot was incubated for 5 min in 12 ml Immun-Star HRP substrate. The HRP blot was then placed in a sheet protector to prevent drying out during imaging. The chemiluminescent HRP blot was imaged first to capture maximum signal intensity.

Blots were imaged with a VersaDoc 4000 using 4 x 4 binning for acquisition. Integration time was 3.5 sec for the Qdot blot and 4 min for the chemiluminescent blot. A 50 mm lens and 655bp20 filter (Omega Optical) were used to image the Qdot 655 blot.

Western Blotting With Qdot Conjugates

C166-GFP mouse endothelial cells stably expressing the GFP gene (obtained from ATCC #CRL-2583) were transfected with siLentFect™ lipid reagent and 5 nM of several siRNA-GFP duplexes that had different predicted knockdown efficiencies: negative control (scramble), siRNA-X, siRNA-Y, and siRNA-Z. Cells were lysed 24 hr posttransfection in Laemmli sample buffer containing 5% β-mercaptoethanol in a total volume of 125 µl and incubated at 85°C for 5 min. Protein was quantitated using an Experion™ Pro260 analysis kit, after which 10–40 µg was separated on Ready Gel® 4–15% Tris-HCl gels and then transferred in Towbin buffer to Immobilon-FL membranes using the Mini Trans-Blot® cell following manufacturer instructions. After transfer, the membrane was incubated in blocking buffer for 1 hr at RT with agitation. The membrane was then incubated for 1 hr in blocking buffer containing 1:400 mouse anti-GAPDH (Ambion, Inc.) and rabbit anti-GFP (BD Biosciences). After three washes with TBST, the blot was incubated for 1 hr in blocking buffer containing 1:1,000 Qdot 605-goat anti-mouse, Qdot 655-goat anti-rabbit, and Qdot 705-streptavidin conjugates. The blot was washed three times in TBST, then three times in TBS. Finally, the blot was imaged with a VersaDoc 4000 imager and emission filters specific to Qdot 605, 655, and 705 (Omega Optical).

Results and Discussion

Optimizing Excitation of QDs

Two factors to consider when selecting an excitation source for QDs are wavelength and power output. Although any light source that emits wavelengths shorter than the emission spectrum of the QD can be used, the extinction coefficient of QDs (and thus the probability that light will be absorbed) is greater at shorter wavelengths (Quantum Dot 2005). Therefore, short wavelengths are generally more efficient and will result in a brighter signal. On the other hand, light sources of greater wavelength can have a higher power output, and in some cases this compensates for the lower extinction coefficient.

The standard excitation source for Molecular Imager FX™ and PharosFX laser scanners is a 532 nm laser, which can excite all QDs with an emission of greater wavelength. An external 488 nm laser is also available. For the PharosFX imager, however, the power output of the 532 nm laser is typically 2-fold greater than that of the 488 nm laser, and this translates to approximately twice the photon density. This large difference in photon density compensates for the lower extinction coefficient, and therefore the standard 532 nm laser is generally satisfactory for all QDs other than those with emission below 532 nm, which must be excited with the 488 nm laser.

The most common excitation source included with CCD imagers, including VersaDoc, ChemiDoc™, and Gel Doc™ imagers, is a broad range UVB lamp, which has a peak wavelength output of 302 nm. This source is suitable for all Qdot QDs we tested. Although UV lamps deliver a low photon density compared to lasers, the VersaDoc imager is still a practical imager for QDs, since 302 nm light is highly efficient in exciting QDs.

Selection of Emission Filters for Detection of Qdot QDs With PharosFX and VersaDoc 4000 Imagers

The performance of QDs in multiplex fluorescence detection largely depends on selection of tools for fluorescence excitation and detection. Standard emission filters of PharosFX (Table 1) and VersaDoc 4000 (Table 2) imagers are suitable for detecting some Qdot QDs. But because these filters are not optimally aligned to the emission peaks of the Qdot QDs, they do not allow the highest possible sensitivity and spectral separation.

The brightest Qdot QDs detected by the PharosFX imager were the 655, 705, and 800 dots; dots with shorter wavelength emission were far dimmer (Figure 1A). Thus, the standard filters are of limited use for 565, 585, and 605 dots. Nonetheless, when the 488 nm laser is used, the PharosFX imager can efficiently distinguish pairs of dots for multiplex applications. Acceptable dot combinations for multiplex detection with standard filters are listed in Table 1. Although visual separation of dot pairs is possible, the low intensity of the Qdot QDs that emit below 655 nm would require the sample being detected to be at relatively high abundance.

As expected, narrow bandpass filters aligned to the emission peaks of the Qdot QDs produced higher sensitivity and better spectral separation. The number of dot combinations acceptable for multiplexing is greater when Qdot-specific filters are used (Table 3). Furthermore, with Qdot-specific filters, all dots were detected when the 488 nm laser was used (Figure 1B). Similar results would be expected when using the 532 nm laser, except 525 dots cannot be used.

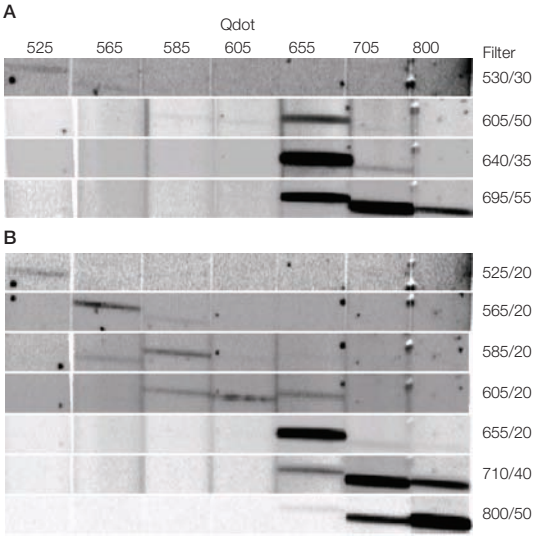

Fig. 1. Detection of Qdot QDs on the PharosFX imager. Qdot QDs with different emission peaks were detected using standard (**A**) or Qdot-specific (**B**) filters.

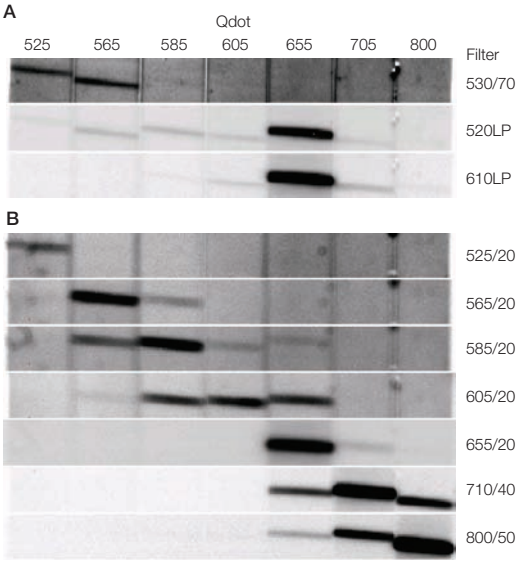

Fig. 2. Detection of Qdot QDs on the VersaDoc 4000 imager. Qdot QDs with different emission peaks were detected using standard (**A**) or Qdot-specific (**B**) filters.

Table 1. Acceptable Qdot combinations for 488 laser excitation and standard PharosFX filters.

Dot 1	Filter 1	Dot 2	Filter 2
525	530/30	655	640/35
525	530/30	705	695/55
525	530/30	800	695/55

Table 2. Acceptable Qdot combinations for UV excitation and standard VersaDoc 4000 filters.

Dot 1	Filter 1	Dot 2	Filter 2
525 or 565	530/70	655	610LP
525 or 565	530/70	705*	610LP
525 or 565	530/70	800*	610LP

* With 660SP filter removed from lens.

Table 3. Acceptable Qdot combinations for 488 nm laser excitation and Qdot-specific filters.

	525	565	585	605	655	705	800
525	—	•	•	•	•	•	•
565	•	—	∘	•	•	•	•
585	•	∘	—	∘	•	•	•
605	•	•	∘	—	∘	•	•
655	•	•	•	∘	—	∘	•
705	•	•	•	•	∘	—	∘
800	•	•	•	•	•	∘	—

• = Optimal combination of Qdot QDs for multiplexing.
∘ = Suboptimal combination of Qdot QDs; some spectral overlap can be observed.

Table 4. Acceptable Qdot combinations for UV excitation and Qdot-specific filters.

	525	565	585	605	655	705	800
525	—	•	•	•	•	•	•
565	•	—	∘	•	•	•	•
585	•	∘	—	∘	•	•	•
605	•	•	∘	—	∘	•	•
655	•	•	•	∘	—	∘	∘
705	•	•	•	•	∘	—	∘
800	•	•	•	•	∘	∘	—

• = Optimal combination of Qdot QDs for multiplexing.
∘ = Suboptimal combination of Qdot QDs; some spectral overlap can be observed.

The VersaDoc 4000 imager excited the shorter wavelength dots more efficiently than the PharosFX imager (Figure 2A). This was expected because of the greater extinction coefficient in the UV spectra by QDs. Due to the transmission ranges of the standard filters, however, only the three dot combinations shown in Table 2 can be dependably distinguished.

As with the PharosFX imager, use of Qdot-specific filters on the VersaDoc imager allows a broader range of dot combinations to be used (Table 4). The intensity of emission of Qdot 525, 565, 585, and 605 upon UV excitation makes them more practical as multiplex partners than they are with visible light excitation (Figure 2B).

Comparison of Sensitivity of Qdot QDs and HRP-Chemiluminescent Labeling of Dot Blots

The sensitivity of protein detection with Qdot conjugates was similar to that with Immun-Star HRP substrate, when normalized to a BSA control (Figure 3A, B), but Qdot QDs displayed better linearity at lower concentrations of protein (Figure 3C). The HRP blot, however, had a lower membrane background signal in the area between wells — more than an order of magnitude lower

than that of the closest Qdot 655 data. Use of low-fluorescence membrane would provide an improvement in the signal-to-background ratio for Qdot blots.

Multiplex Western Blotting With an Internal Standard for Better Quantitation

Multiplex western blotting can be used to verify that an equal quantity of protein is being loaded onto each lane of the gel, e.g., by probing a housekeeping protein along with the antigen of interest in each sample. This is important for quantitative applications. Such an experiment is shown in Figure 4. Expression levels of Green Fluorescent Protein (GFP) in a stably transfected cell line were altered using siRNA from the GFP gene. Glyceraldehyde-3-phosphate dehydrogenase (GAPDH) was chosen as an internal standard. Probing the blot with antibodies for both antigens allowed normalization of GFP expression. As shown in Figure 4, expression levels of GFP were quite different when comparing direct GFP volume values to those normalized to the GAPDH volume values.

According to the uncorrected data, the treatment with siRNA-Z produced the least efficient silencing (highest value of GFP concentration on the blot) of the GFP gene. However, the normalized data shows that the treatment with siRNA-Z ranked third of the four treatments in the extent of downregulation of the GFP expression, with least efficient silencing observed in the control treatment.

Conclusions

Fluorescent nanoparticles such as Qdot QDs can serve as excellent visualization labels for multiplex western blotting. Qdot QDs provided higher data quality than chemiluminescent blotting, due to better linearity at low concentrations of antigen, and the capability of using internal standards on the same blot.

The versatile functionality and optimized fluorescence detection of the VersaDoc 4000 and PharosFX systems can be used to image QD-labeled, multiplex western blots with detection sensitivity equivalent to that of chemiluminescence detection.

Acknowledgements

We thank Marcel Bruchez (Invitrogen Corporation) for Qdot materials and technical consultations, and Teresa Rubio (Bio-Rad) for applications related to RNAi methods and samples for western blotting.

References

Alivisatos AP, Semiconductor clusters, nanocrystals, and quantum dots, Science 271, 933–937 (1996)

Bio-Rad Laboratories, Inc., Protein blotting guide, Bio-Rad bulletin 2895

Chan WC and Nie SM, Quantum dot bioconjugates for ultrasensitive nonisotopic detection, Science 281, 2016–2018 (1998)

Kurien BT and Scofield RH, Protein blotting: a review, J Immunol Methods 274, 1–15 (2003)

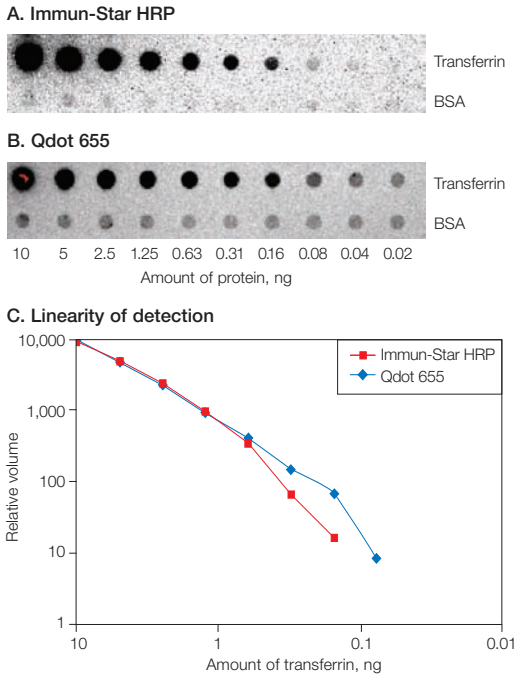

Fig. 3. Comparison of chemiluminescence and Qdot fluorescence. Dot blots were labeled with Immun-Star HRP (**A**) or Qdot 655 (**B**) and imaged with a VersaDoc 4000 imager. Integration time was 4 min for Immun-Star HRP and 3.5 sec for Qdot 655. **C**, plot of relative dot volume vs. amount of loaded protein. R^2 values were 0.9968 for Immun-Star HRP, 0.9992 for Qdot 655.

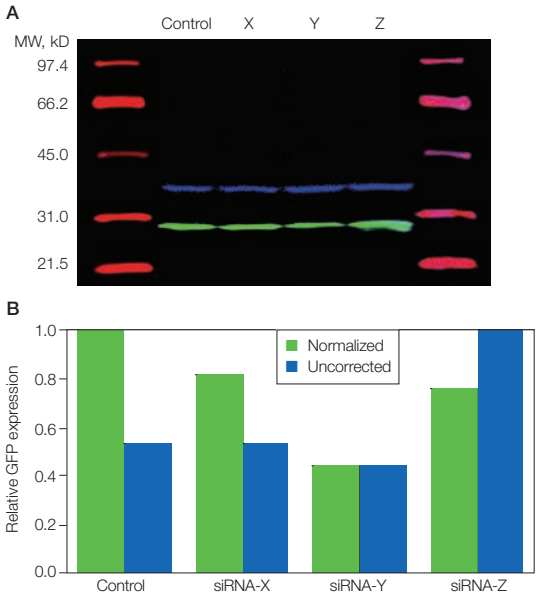

Fig. 4. Multiplex western blot detection of GAPDH and GFP expression in C166-GFP endothelial cells. Cells were transfected with four different siRNA-GFPs (X, Y, Z, or a scrambled control). **A**, visualization using the Qdot-conjugated antibodies to GFP (green), GAPDH (blue), and biotinylated protein standards (red) described in Methods. The image was acquired with a VersaDoc 4000 imager using QD-specific emission filters. **B**, GFP expression relative to GAPDH. GFP expression levels from the blot were corrected for variations in protein loading and transfer using a correction factor F, where $F = [GAPDH_{control}]/[GAPDH_x]$, and x refers to lanes X, Y, or Z of the blot. Normalized GFP expression is then [GFP]/F.

Quantum Dot Corporation, Qdot nanocrystals, http://www.qdots.com/live/render/content.asp?id=84 (2005)

Renart J et al., Transfer of proteins from gels to diazobenzyl-oxymethyl-paper and detection with antisera: a method for studying antibody specificity and antigen structure, Proc Natl Acad Sci USA 76, 3116–3120 (1979)

Towbin H et al., Electrophoretic transfer of proteins from polyacrylamide gels to nitrocellulose sheets: procedure and some applications, Proc Natl Acad Sci USA 76, 4350–4354 (1979)

Wu X et al., Immunofluorescent labeling of cancer marker Her2 and other cellular targets with semiconductor quantum dots, Nat Biotechnol 21, 41–46 (2003)

Use of the Bio-Plex™ Cytokine Immunoassay to Determine Cytokine Expression Levels in the Intestinal Mucosa

Daniel R Clayburgh and Jerrold R Turner, Department of Pathology, The University of Chicago, Chicago, IL 60637 USA

Introduction

The intestinal tract is a major interface between the finely regulated internal milieu of the body and the external environment. As such, the intestine has a highly developed and specialized mucosal defense system, composed of the epithelial barrier and the intestinal immune system. The intestine faces an enormous, constant antigenic load, both from bacteria and food antigens; however, only a small minority of antigens in the gut represent a threat requiring immune activation and inflammation. Thus, the intestinal immune system is finely regulated to respond appropriately to either harmful or benign antigens (Sansonetti 2004).

Cytokine signaling between the various immune cells is an important facet of immune system regulation; thus, determining the cytokine profile of the intestinal mucosa is important in understanding intestinal immune responses. Multiplex cytokine analysis offers the ability to assay a broad array of cytokines in a single sample; however, this technology has not previously been applied to the study of cytokine expression within the mucosa of the intestine. The goal of this study was to explore the use of the Bio-Plex cytokine assay system for the determination of cytokine levels in the intestinal mucosa. We examined cytokine expression in control mice and in mice treated with anti-CD3, which elicits systemic T-cell activation (Ferran et al. 1990) and diarrhea (Clayburgh et al. 2005), and found that the Bio-Plex system is easily adapted to assess cytokine profiles in the intestinal mucosa.

Methods

Animals

Eight-week-old C57BL/6 mice were injected intraperitoneally with 200 µg of anti-CD3 or phosphate-buffered saline (PBS). Three hours after injection, mice were euthanized for organ harvest. All animal procedures were approved by the Institutional Animal Care and Use Committee at the University of Chicago.

Tissue Harvest and Cell Lysis

Each mouse was euthanized and ~1.5 cm sections of ileum were removed. The ileum was then cut into ~3 mm^3 pieces and placed in a 1.5 ml Eppendorf tube containing 500 µl of lysing solution (Bio-Plex cell lysis kit). Samples were ground using a microtube pestle and then frozen at –80°C. After thawing, samples were sonicated on ice using three short pulses (<3 sec) from a Sonifier unit model 250 (Branson Ultrasonics Corporation). Samples were then centrifuged at 4,500 x g for 6 min at 4°C. The supernatant was transferred to a fresh tube, and the protein concentration was determined using a *DC*™ protein assay kit. The protein concentration of each sample was adjusted to 500 µg/ml with lysing solution, aliquoted, and stored at –20°C.

Multiplex Analysis

A Bio-Plex assay for 23 mouse cytokines (IL-1α, IL-1β, IL-2, IL-3, IL-4, IL-5, IL-6, IL-9, IL-10, IL-12 (p40), IL-12 (p70), IL-13, IL-17, eotaxin, G-CSF, GM-CSF, IFN-γ, KC, MCP-1 (MCAF), MIP-1α, MIP-1β, RANTES, TNF-α) was run according to the recommended procedure. Briefly, a standard curve was created via dilution of premixed standards to 50,000 pg/ml, followed by serial dilution to 8 concentrations ranging from 32,000 to 1.95 pg/ml. The assay was performed in the 96-well filtration plate supplied with the Bio-Plex kit. Premixed beads coated with target antibodies (50 µl) were added to each well, and then washed twice with Bio-Plex wash buffer. Premixed standards or undiluted samples (50 µl) were then added to the wells, followed by shaking at 1,100 rpm for 30 sec and incubation for 30 min with shaking at 300 rpm at room temperature. Wells were then washed 3 times with Bio-Plex wash buffer, and 25 µl of the premixed detection antibodies was added to the wells. This was followed by shaking at 1,100 rpm for 30 sec and incubation for 30 min with shaking at 300 rpm at room temperature. Wells were again washed 3 times with Bio-Plex wash buffer, and 50 µl of streptavidin-PE was added to the wells. This was incubated for 10 min with shaking at 300 rpm. Wells were washed 3 times with Bio-Plex wash buffer, and the beads were resuspended in 125 µl Bio-Plex assay buffer. The samples were then read using the Bio-Plex suspension array system, and the data were analyzed using Bio-Plex Manager™ software with 5PL curve fitting.

Results and Discussion

The results of the Bio-Plex analysis of ileal mucosa from control and anti-CD3-treated animals are shown in Figure 1. The Bio-Plex system effectively detected cytokines across a broad range of concentrations, from ~1.5 pg/mg total protein to

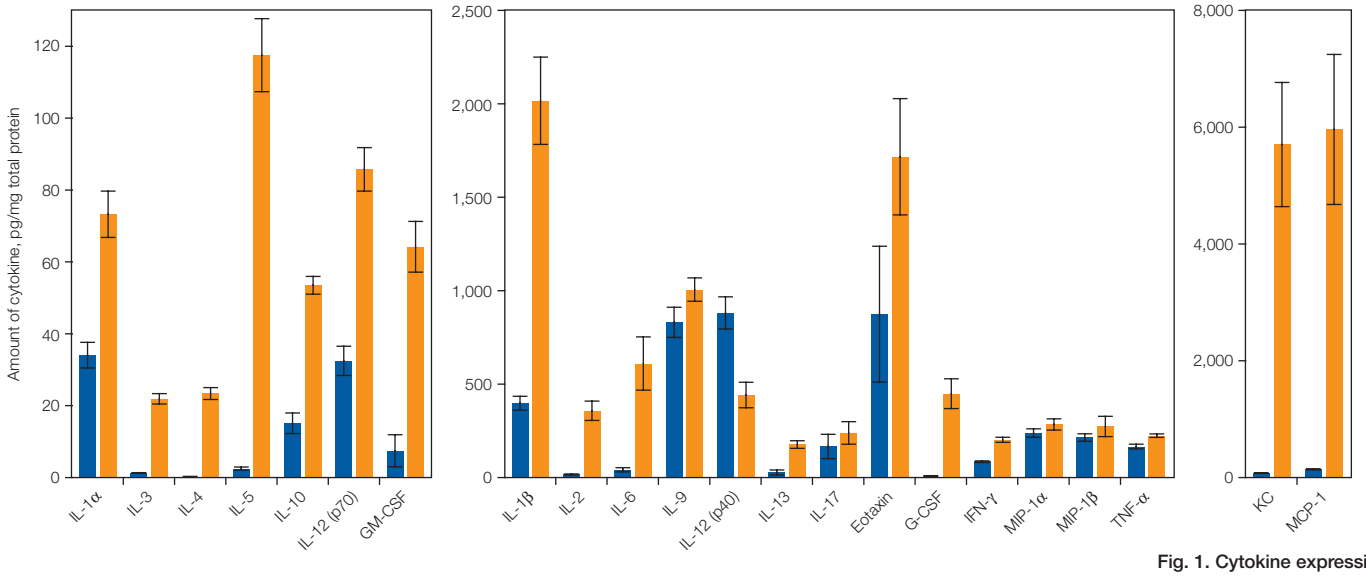

Fig. 1. Cytokine expression in ileal mucosa from control (■) and anti-CD3-treated mice (■). RANTES values were below the level of reliable detection.

over 15,000 pg/mg total protein. As expected, anti-CD3 treatment resulted in significantly increased expression of most cytokines tested, including IL-1α, IL-1β, IL-2, IL-3, IL-4, IL-5, IL-6, IL-10, IL-12 (p70), IL-13, IL-17, eotaxin, G-CSF, GM-CSF, IFN-γ, KC, MCP-1 (MCAF), MIP-1α, MIP-1β, and TNF-α, based on Student's *t*-test.

Conclusions

In this study we have demonstrated the successful determination of expression levels of multiple cytokines within the intestinal mucosa using the Bio-Plex suspension array system. In agreement with previous reports, we found greatly increased expression of numerous cytokines within the mucosa in mice injected with anti-CD3. This procedure should prove important for the analysis of changes within the intestinal immune system during disease or treatment protocols.

References

Clayburgh DR et al., Epithelial myosin light chain kinase-dependent barrier dysfunction mediates T cell activation-induced diarrhea in vivo, J Clin Invest 115, 2702–2715 (2005)

Ferran C et al., Cytokine-related syndrome following injection of anti-CD3 monoclonal antibody: further evidence for transient in vivo T cell activation, Eur J Immunol 20, 509–515 (1990)

Sansonetti PJ, War and peace at mucosal surfaces, Nat Rev Immunol 4, 953–964 (2004)

For additional copies of this article, request bulletin 5374.

FAST PCR

The polymerase chain reaction (PCR) has traditionally been optimized for specificity and, to a lesser extent, product yield. The speed with which the reaction is completed has been of secondary importance.

The availability of software to aid in primer and PCR product design, as well as the use of reagents that can tolerate a range of reaction conditions, has allowed researchers to focus on maximizing throughput by minimizing PCR cycling times.

Some manufacturers have recently introduced instruments and consumables that are targeted to those performing "fast PCR" — a PCR protocol completed in less than half the typical 90 min. Although many researchers assume that fast PCR is only obtainable through the purchase of these specialized, faster ramping thermal cyclers, in this article, we demonstrate that most of the time savings in fast PCR are achieved simply by modifying thermal cycling conditions.

We present general considerations for accomplishing fast PCR without a specialized thermal cycler and demonstrate that with conventional instruments, reagents, and reaction vessels it is possible to:

- Shorten run times for standard PCR from around 90 to 35 min
- Reliably amplify long targets (1–20 kb) 3- to 4-fold faster than with standard protocols
- Obtain real-time quantitative PCR (qPCR) data with SYBR Green or TaqMan chemistries in under an hour

Authors: Daniel Sullivan, Babette Fahey, and David Titus,
Bio-Rad Laboratories, Inc., Hercules, CA 94547 USA

Saving Time at Each Step of a PCR

Standard PCR protocols for amplifying targets of less than 1,000 bp comprise several steps, each of which can be modified to shorten overall run times. Overall reaction time for conventional PCR can be reduced from about 90 min to under 35 min by shortening hold times and by minimizing the temperature differential between one step and the next (Figure 1). Some simple considerations for shortening run times are provided in the sidebar on page 19. The rationale for each of these modifications is explained below.

Initial Denaturation

The first step in the PCR is generally performed at 94–96°C for 2–20 min. This step denatures the initial template into single-stranded DNA and also activates hot-start polymerases. While 2–3 min at 94–95°C is usually sufficient to fully denature total genomic DNA, some hot-start polymerases require 15 or 20 min at 95°C to be activated. When using an antibody-modified hot-start polymerase such as iTaq™, however, both activation and initial denaturation can be accomplished in just 15–30 sec at 98°C (Figure 2). These parameters can also work well for qPCR, with no deleterious effects on reaction efficiencies or C_T values over a range of target concentrations (data not shown).

Denaturation While Cycling

The hold times and temperatures required to denature the template during PCR cycling are not as stringent as in the initial denaturation step, because the template being denatured is a PCR product, which is usually much shorter and less complex than the initial template DNA. We have found that a 1 sec denaturation at 92°C is sufficient for a variety of PCR products amplified with iQ™ supermix, including the 83.5% GC, 505 bp PCR product in Figures 1 and 2, as well as a 64% GC, 150 bp PCR product in lambda DNA (data not shown). This is consistent with the observation of Yap and McGee (1991) that temperatures above 92°C are unnecessary for denaturing PCR products shorter than 500 bp.

GENERAL CONSIDERATIONS FOR MINIMIZING RUN TIMES AND MAXIMIZING THROUGHPUT

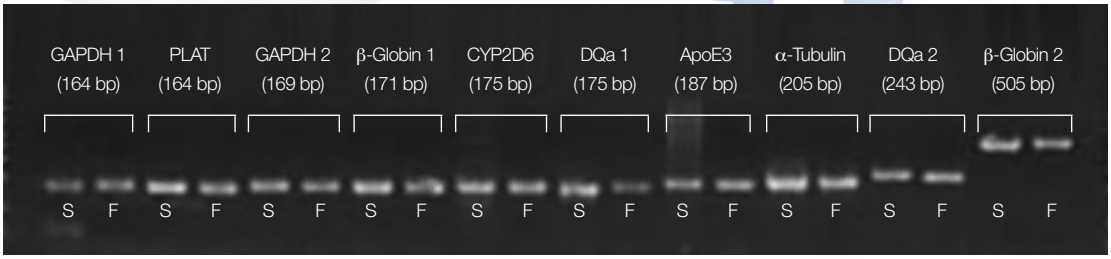

Fig. 1. Reactions run in less than 35 min generate results comparable to those run in 90 min. S, standard protocol: 95°C for 3 min, then 35 cycles of 95°C for 15 sec, 60°C for 30 sec, and 72°C for 30 sec, followed by 72°C for 10 min. Actual run time, 88 min. F, fast protocol: 98°C for 30 sec, then 35 cycles of 92°C for 1 sec and 70°C for 15 sec, followed by 72°C for 1 min. Actual run time, 32 min. All amplicons were designed with primer T_m = 68–72°C. Each 20 µl reaction contained 2,000 human genome targets.

Annealing and Extension

Because most polymerases are highly active in the temperature range typical for primer annealing (55–70°C), the annealing and extension steps of a PCR protocol can often be consolidated into a single step. Using a two-step PCR protocol rather than the standard three-step protocol can result in a significant reduction in run time. Further reductions can be achieved by reducing the incubation time of this combined annealing/extension step. The standard annealing times (15–60 sec) and extension times (1 min per kb of PCR product) are, in most instances, unnecessarily long. Because primer concentrations are high relative to template, annealing of primers requires just a few seconds at the optimal reaction temperature. Furthermore, a well-optimized reaction using iTaq polymerase can amplify PCR products efficiently with much shorter extension times. As shown in Figure 1, a 15 sec combined annealing/extension incubation can be sufficient for PCR products up to 500 bp. Even shorter extension times are possible with iProof™ polymerase, which can amplify a 2 kb target with an annealing/extension time under 15 sec.

It is important to optimize the annealing/extension temperature, because it is the major determinant of specificity of the reaction. If the annealing temperature is too high, the primers will not anneal efficiently, resulting in no amplification or poor yield; if it is too low, primer mismatches and nonspecific amplification may occur, and yield may be diminished (Rychlik et al. 1990). To maximize both speed and specificity, use the highest possible annealing temperature without sacrificing adequate reaction yield. Gradient-enabled thermal cyclers allow optimization of the annealing temperature in a single run.

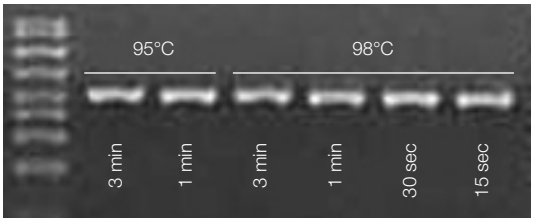

Fig. 2. Initial denaturation and enzyme activation time requires 30 sec or less with iQ supermix, which uses iTaq hot-start polymerase. Gel image shows a 505 bp β-globin target amplified using iTaq polymerase with a range of initial denaturation conditions. Protocol included initial denaturation conditions as shown, then 35 cycles of 92°C for 1 sec and 68°C for 15 sec, followed by 72°C for 1 min. Actual run time, 34–38 min.

To establish general considerations for choosing primers and annealing/extension temperatures for fast PCR, we performed a series of reactions using a range of annealing/extension temperatures and a panel of primer pairs that had average T_m values varying from 58 to 72°C. Figure 3 shows that a range of annealing/extension

Testing Assumptions

How Much Does a Cycler's Ramp Rate Affect PCR Run Time?

Many researchers assume that substantial reduction of PCR run times can be achieved only by using specialized thermal cyclers with faster ramp rates. To test this idea, we ran the same two-step protocol on three thermal cyclers with differing ramp rates — the iCycler (maximum ramp rate, 3.3°C/sec), the MyCycler™ (2.5°C/sec), and a competitor's "fast" thermal cycler (5°C/sec). As shown in the chart at right, the time saved by using a protocol optimized for fast PCR is substantial (56–65 min), whereas the additional time saved by a faster-ramping cycler is relatively small (6–8 min). These time savings should be weighed against the extra cost and inflexibility of faster-ramping cyclers in terms of consumables, reagents, and range of thermal cycling applications.

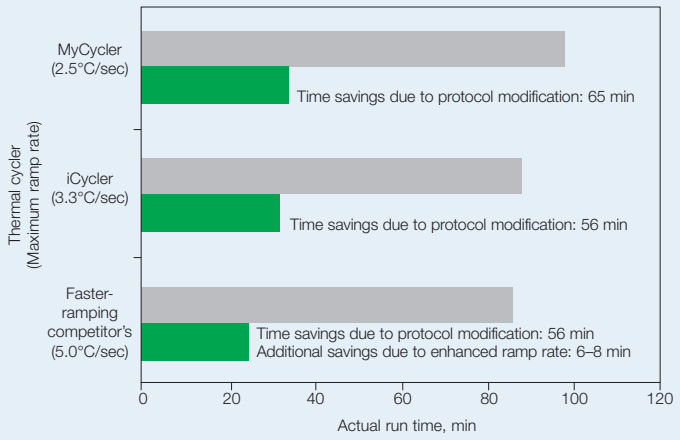

Run time savings from protocol modification vs. faster ramping. Actual run times were measured for three thermal cyclers with different ramp rates running a standard (■, three-step) protocol and a modified fast (■, two-step) protocol. Standard protocol was 95°C, 3 min; then 35 cycles of 95°C, 15 sec; 60°C, 30 sec; and 72°C, 30 sec; then 72°C, 10 min. Fast protocol was 98°C, 30 sec; then 35 cycles of 92°C, 1 sec and 70°C, 15 sec; then 72°C, 1 min. Ramp rate for competitor is compared with the iCycler and MyCycler.

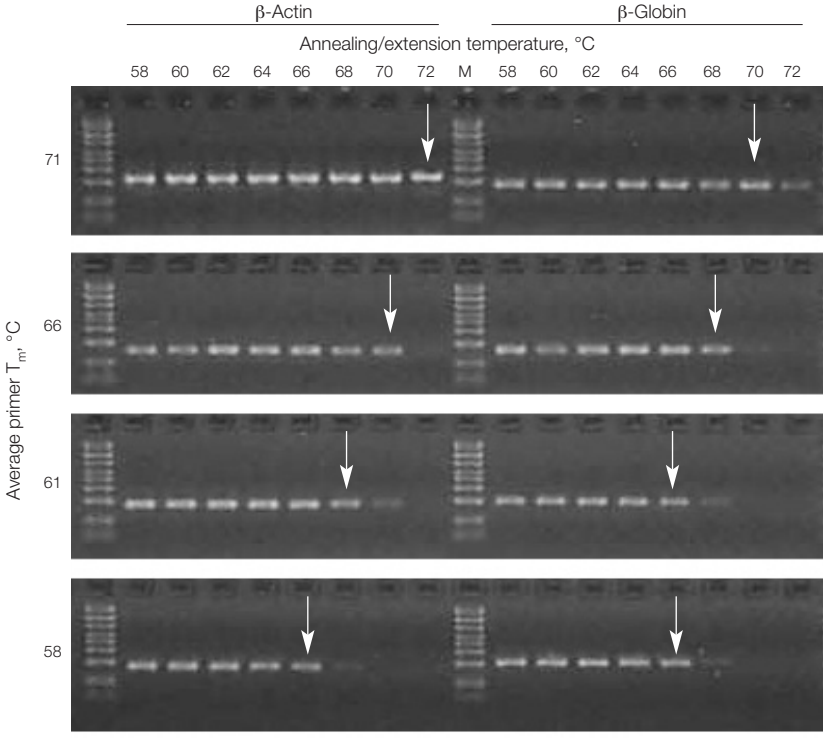

Fig. 3. Determining the optimal annealing and extension temperature for fast PCR. The cycling protocol was 98°C, 30 sec; then 35 cycles of 92°C, 1 sec and annealing/extension temperature, 15 sec; then 72°C, 1 min. Actual run time, 33–42 min. Arrows indicate the reaction conditions that provided the shortest ramp times and highest specificity while maintaining good yield.

temperatures worked well for fast PCR. The fastest overall reaction times for each primer pair were obtained by using the highest annealing/extension temperature that generated a good band on the gel (i.e., strong intensity, single product). See sidebar on the next page for the simple considerations derived from these experiments.

Note: If you choose to redesign primers for faster PCR reactions, many primer design programs (e.g., Primer3 software*) simplify design by allowing you to specify the desired primer T_m. Existing primers with low T_m values can often be easily adapted to faster PCR by adding 2–4 bases to the 5' ends. Naturally, such primer modifications must be checked for new self- and cross-primer complementarity.

Ramping Time

Ramping time is the time required by the thermal cycler to transition from one incubation temperature to another. Two parameters contribute to ramping time — the ramp rate of the cycler and the difference between consecutive temperatures. Smaller temperature excursions result in shorter ramping times. While the contribution of ramp rate to overall cycling time has been highlighted by manufacturers of faster-ramping thermal cyclers, the time saved by using these specialized cyclers is relatively minor (6–8 min) compared to the savings gained from optimizing thermal cycling parameters for speed (56–65 min; see sidebar at top of page).

As described above, cycling time can also be reduced by converting from a three-step to a two-step protocol in which the annealing and extension steps are combined at a temperature optimal for primer annealing yet sufficient for primer extension. Such two-step PCR protocols generate yields similar to three-step protocols for products up to 200 bp (Cha and Thilly 1995). Furthermore, a combined annealing and extension step at 60°C is typical for qPCR assays using TaqMan probes, and reaction efficiencies of around 100% are routinely achieved for such assays. This suggests that the processivity of *Taq* at this lower temperature is sufficient to fully extend products of 70–200 bp.

* This product includes software developed by the Whitehead Institute for Biomedical Research.

Final Extension

A post-PCR final incubation step of 5–10 min at 72°C is often recommended to promote complete synthesis of all PCR products. Although this is commonly referred to as an extension step, a major purpose is to allow reannealing of the PCR product into double-stranded DNA so it can be visualized using ethidium bromide after gel electrophoresis or used for cloning. We found that this step can be shortened to 30–60 sec for PCR products of 100–1,000 bp (Figure 4).

Number of Cycles

PCR can be completed in relatively few cycles (<20) if the starting target concentration is high. When starting with lower copy numbers (e.g., 100 copies) of target DNA, 35 cycles of PCR are generally adequate to detect the resulting product on a gel stained with ethidium bromide. With less starting target, additional cycles may be necessary. In practice, the amount of target is often unknown and may be only a few hundred copies per reaction. For this reason, researchers usually prefer to run 30–45 cycles of PCR despite the potential time savings of running fewer cycles.

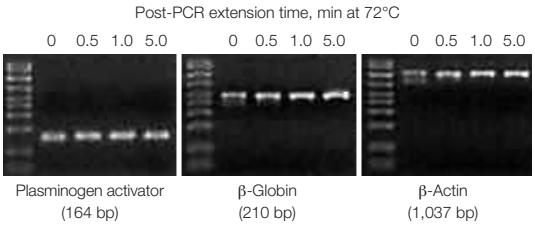

Fig. 4. The final extension step can be reduced to 1 min or less. Targets of 164–1,037 bp were amplified from human genomic DNA using a fast PCR protocol, then a final step of 0–5 min at 72°C was performed before gel analysis. Cycling protocol for 164 bp PCR product: 98°C, 30 sec; then 35 cycles of 92°C, 1 sec and 68°C, 15 sec. Actual run time, 33–38 min. Cycling protocol for 505 and 1,037 bp PCR products: 98°C, 30 sec; then 35 cycles of 92°C, 1 sec and 68°C, 30 sec. Actual run time, 41–46 min.

Fast Real-Time qPCR

Our guidelines for fast PCR can be applied to other PCR applications, including real-time qPCR. For qPCR, primers are usually designed to amplify relatively short targets (70–200 bp) to ensure maximum efficiency. Such short targets may not require long denaturation and extension times, making them particularly suitable for modification for fast PCR assays without the need for special reagents, plastics, or instrumentation.

SYBR Green I Chemistry

Bio-Rad has traditionally recommended using a two-step, rather than a three-step, protocol for any real-time qPCR using SYBR Green chemistry. Run times can be further shortened by minimizing hold times using the same considerations used for conventional PCR. Figure 5 shows data from a

General Considerations for Fast PCR

Protocol

- Begin with this fast PCR protocol template: 98°C, 30 sec; then 35 cycles of 92°C, 1 sec and 70°C, 15 sec; then 72°C, 1 min
- Modify the annealing/extension temperature so that it is halfway between 72°C and the average of the primer T_m values; for example, if the average primer T_m is 58°C, use an annealing/extension temperature of 65°C
- Alternatively, employ the rapid optimization strategy (below) that uses temperature gradients to optimize both speed and specificity
- If the starting target number might be <100 copies, perform 40 cycles

Reaction Mix

- For targets <1 kb, use an antibody-mediated hot-start polymerase such as iTaq; for targets >1 kb, use highly processive iProof polymerase
- If using existing primers, verify that T_m values are in the range of 58–72°C; if designing new primers, specify T_m values near 70°C*

DNA Amplicon Size

Any size PCR product up to 20 kb can be amplified using these fast PCR guidelines. For fastest reactions, however, amplify targets <250 bp.

Rapid Optimization Strategy for Fast PCR

This simple strategy can quickly optimize a PCR reaction for minimal hold times, minimal ramping time, and shortest overall run times.

- Begin with this fast PCR protocol template: 98°C, 30 sec; then 35 cycles of 92°C, 1 sec, xx°C, 15 sec; then 72°C, 1 min, where xx = temperature gradient (see below)
- Use a temperature gradient (e.g., 0–10°C above the lowest primer T_m) to find the highest possible annealing/extension temperature
- Perform a second run with a temperature gradient (e.g., 85–95°C) to find the lowest possible denaturation temperature during cycling

Example:

Optimization Stage	PCR Protocol	Run Time
Before optimization	95°C, 3 min; then 35 cycles of 95°C, 15 sec, 60°C, 30 sec, 72°C, 30 sec; then 72°C, 10 min	88 min
Hold times reduced and annealing and extension steps combined using guidelines	98°C, 30 sec; then 35 cycles of 95°C, 1 sec, 60°C, 15 sec; then 72°C, 1 min	60 min
Gradient used to minimize temperature excursions	98°C, 30 sec; then 35 cycles of 90°C, 1 sec, 65°C, 15 sec; then 72°C, 1 min	36 min

Troubleshooting Fast PCR

Symptom	Recommendation
Weak gel band	Increase the annealing/extension time in 5 sec increments Lower the annealing/extension temperature by 2 or 4°C Raise the denaturation temperature by 1 or 2°C
Nonspecific bands	Raise the annealing/extension temperature by 2 or 4°C Redesign primers to have 2–4°C higher T_m values, or to amplify a different region of the target sequence

* We recommend designing and verifying primer T_m values with a calculator such as Primer3 (http://frodo.wi.mit.edu/cgi-bin/primer3/primer3_www.cgi) (Rozen and Skaletsky 2000), which references the thermodynamic parameters of Breslauer et al. (1986) and Rychlik et al. (1990). The various oligo T_m calculators available on web sites can give quite different T_m values for the same oligonucleotide.

modified real-time qPCR assay of a lambda DNA PCR product using iQ™ SYBR® Green supermix. In this assay, primer concentrations were increased to 0.75 µM. As this figure illustrates, it is possible to obtain reproducible results, minimal variance around the standard curve, and reaction efficiencies close to 100% for real-time PCRs completed in under 40 min.

For SYBR Green assays, we recommend running a post-amplification melt-curve analysis. This will lengthen the overall run time by approximately 10 min, but will provide valuable data on reaction specificity. The presence of a single product in the melt-curve analysis (Figure 5C) indicates the high specificity of the reaction.

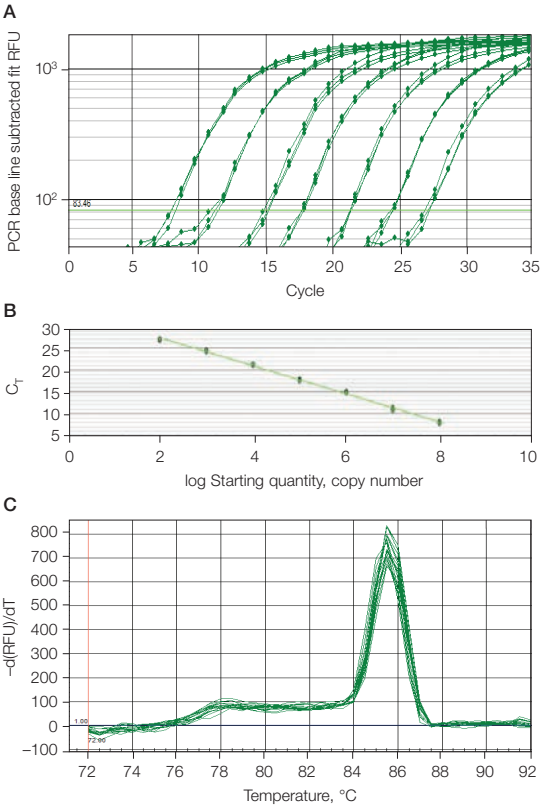

Fig. 5. SYBR Green real-time qPCR completed in under 40 min. Fluorescence curves (**A**), standard curve (**B**), and melt curves (**C**) are shown for a 150 bp region amplified from lambda DNA. Standard curve had y = –3.209x + 33.380, R^2 = 0.998; PCR efficiency = 104.9%. Cycling protocol was 98°C, 30 sec; then 35 cycles of 92°C, 1 sec and 70°C, 15 sec; then melt curve. Actual qPCR time, 37 min, 38 sec. Total run time with melt curve, 47 min, 36 sec.

Dual-Labeled Probes

Quantitative PCR using dual-labeled probes (often called TaqMan or 5' nuclease assays) uses a two-step PCR protocol with a combined annealing and extension step, commonly performed at 60°C. A combined annealing and extension step is necessary because the fluorescent chemistry requires the probe to be annealed to its target while the product is being extended. Again, significant run time reductions can be made simply by reducing hold times at each step. Table 1 shows data from a TaqMan real-time qPCR run under three different thermal cycling conditions. These real-time PCRs used iTaq supermix with ROX and were performed on the iQ™5 system, which has a maximum ramp rate of 3.3°C/sec. The unmodified protocol used manufacturer-recommended reaction conditions and yielded a run time of 68 min. Run time was reduced to 61 min when the reaction was run using a competitor's fast PCR protocol, which is designed for use with their reagents and instruments specialized for fast PCR. Using a faster protocol achieved a further reduction of 15 min, resulting in an overall run time of 46 min. This protocol used a 30 sec initial denaturation and enzyme activation step at 98°C, and reduced hold times during cycling — 1 sec at 92°C for denaturation and 15 sec for annealing and extension. Each of these runs produced virtually identical results, with the maximum difference in average C_T between runs being 0.5 or less.

Saving Time in Long PCR

In general, longer targets (above 1 kb) need longer extension times, resulting in runs that can last several hours. The extremely high processivity of iProof polymerase (see sidebar on the next page) enables extension to be completed in much less time and with less enzyme than is required for other polymerases. Elevated annealing temperatures (T_m + 3°C for oligonucleotides >20 bp) are recommended for iProof polymerase due to the

Table 1. Real-time qPCR with dual-labeled probes completed in under an hour. Results are shown for real-time PCR assays using dual-labeled probes. Identical reactions amplifying β-actin from human liver cDNA using iTaq supermix with ROX were run on the iQ5 real-time system using different thermal cycling conditions.

	Unmodified Protocol	Competitor's Fast Protocol	Modified Faster Protocol
Protocol	95°C, 3 min; then 40 cycles of 92°C, 10 sec and 60°C, 30 sec	95°C, 20 sec; then 40 cycles of 92°C, 3 sec and 60°C, 30 sec	98°C, 30 sec; then 40 cycles of 92°C, 1 sec and 60°C, 15 sec
Actual run time	68 min	61 min	46 min
Standard curve equation	y = –3.445x + 24.647	y = –3.376x + 24.895	y = –3.396x + 24.880
R^2 value	1.000	0.998	0.999
Reaction efficiency	95.1%	97.8%	97.0%
C_T values* Concentration			
1 x 10^{-3}	35.08 ± 0.107	34.82 ± 0.475	34.88 ± 0.267
1 x 10^{-2}	31.52 ± 0.097	31.83 ± 0.282	31.67 ± 0.132
1 x 10^{-1}	27.92 ± 0.031	28.34 ± 0.107	28.42 ± 0.272
1 x 10^{0}	24.71 ± 0.054	24.89 ± 0.066	25.02 ± 0.175
1 x 10^{1}	21.27 ± 0.066	21.58 ± 0.049	21.50 ± 0.146
1 x 10^{2}	17.71 ± 0.113	18.03 ± 0.022	17.93 ± 0.127

* Mean C_T ± SD for 3 or more replicates.

iProof Sso7d Technology — Speed, Accuracy, Length, and Reliability

Historically, PCR polymerases provided either high fidelity or high processivity, but not both. Now, using patented* Sso7d fusion technology, Bio-Rad has incorporated both these parameters into a single enzyme: iProof high-fidelity DNA polymerase. This novel polymerase accurately and efficiently amplifies a wide range of DNA templates for use in a variety of applications.

Sso7d Fusion Technology Powers iProof Polymerase

A novel high-fidelity DNA polymerase was engineered and fused to Sso7d, a 63 amino acid dsDNA-binding protein that exhibits no sequence preference. Sso7d gives the polymerase a sliding grip on the minor groove of the replicated DNA, dramatically increasing processivity without compromising catalytic activity or enzyme stability. This technology improves speed, robustness, product length, and tolerance of PCR inhibitors.

Speed and Product Length

iProof DNA polymerase has several major advantages over traditional PCR enzymes. The enhanced processivity conferred by Sso7d results in dramatically reduced extension steps and overall reaction times. With iProof polymerase, extension times for typical targets are reduced to 15–30 sec/kb, and overall reaction times for long targets (2–20 kb) are reduced by 3- to 4-fold (see Figure 6). Furthermore, long and accurate PCR is possible — fragments up to 37 kb can be amplified from low-complexity DNA, and 28 kb fragments can be amplified reliably from human genomic DNA.

Accuracy

iProof polymerase's fidelity is the highest available in a thermostable polymerase; it is 52-fold more accurate than *Taq*. Robust amplification and high yields can be achieved with 2- to 4-fold less enzyme (0.25–1 U/reaction) than other polymerases, making iProof a cost-effective alternative for many applications.

Reliability

The improved polymerase processivity also leads to increased tolerance of PCR inhibitors such as salts and blood components, which are substantial obstacles in forensic and medical sample processing. The Sso7d fusion technology also enhances the performance of SYBR Green real-time qPCR, especially for longer PCR products.

* US patent 6,627,424 and patents pending.

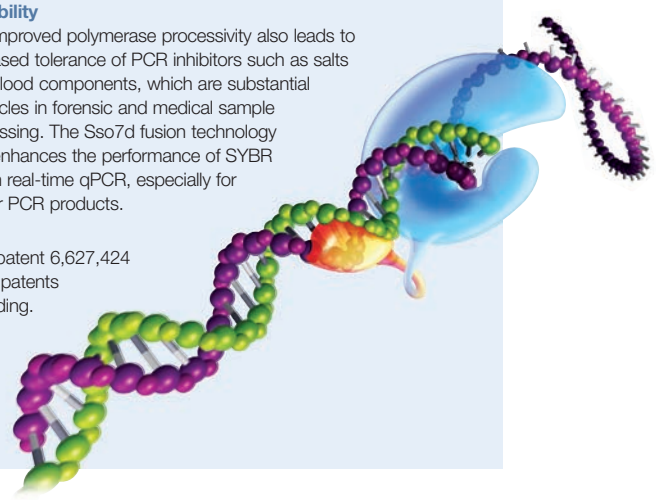

iProof polymerase. Fusion of the dsDNA binding protein Sso7d to an engineered high-fidelity polymerase gives iProof a powerful sliding grip on the replicated DNA.

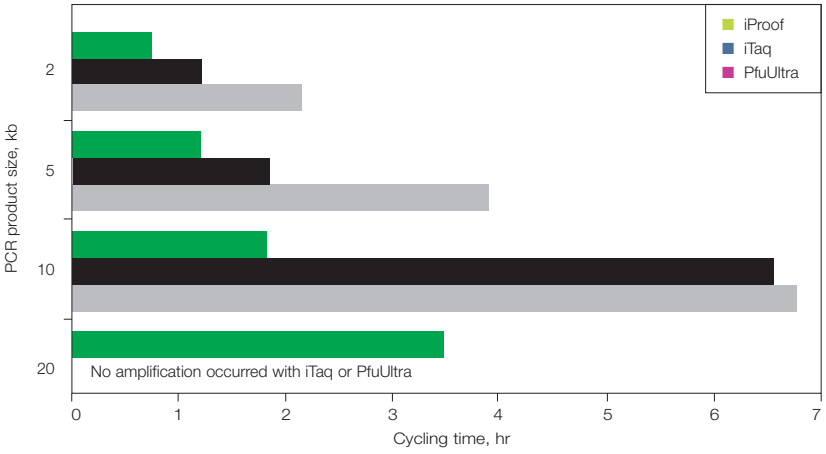

Fig. 6. Long PCR (up to 20 kb) can be achieved 3–4 times faster using iProof polymerase. Targets were amplified from lambda DNA using different polymerases. Primers were designed with T_m = 70–72°C, so that manufacturer-recommended protocols could be converted to two-step protocols. Protocols were run using a range of annealing/extension times; the fastest run time that produced a successful result (based on agarose gel electrophoresis) is plotted.

higher salt concentration in the reaction buffer, so two-step protocols are routinely performed with this enzyme. Figure 6 compares the results of long PCR (2–20 kb) using iTaq, iProof, and PfuUltra polymerases in a two-step protocol with the manufacturer's recommended conditions. Time savings of up to 3- to 4-fold, as well as increased reaction success, were obtained with iProof polymerase.

References

Breslauer KJ et al., Predicting DNA duplex stability from the base sequence, Proc Natl Acad Sci USA 83, 3746–3750 (1986)

Cha RS and Thilly WG, Specificity, efficiency, and fidelity of PCR, pp 37–52 in Dieffenbach CW and Dveksler GS (eds), PCR Primer: A Laboratory Manual, Cold Spring Harbor Laboratory Press, Cold Spring Harbor, NY (1995)

Rychlik W et al., Optimization of the annealing temperature for DNA amplification in vitro, Nucleic Acids Res 18, 6409–6412 (1990)

Rozen S and Skaletsky HJ, Primer3 on the WWW for general users and for biologist programmers, pp 365–386 in Misener S and Krawetz S (eds), Bioinformatics Methods and Protocols: Methods in Molecular Biology, Humana Press, Totowa, NJ (2000); source code available at http://fokker.wi.mit.edu/primer3/

Yap EP and McGee JO, Short PCR product yields improved by lower denaturation temperatures, Nucleic Acids Res 19, 1713 (1991)

Transfection of Caco-2 Cells With siRNA Using the siLentFect™ Lipid Reagent

Daniel R Clayburgh and Jerrold R Turner, Department of Pathology, The University of Chicago, Chicago, IL 60637 USA

Introduction

The tight junctions between intestinal epithelial cells are an important component of the permeability barrier separating the potentially harmful contents of the intestinal lumen from the internal milieu. Cultured monolayers of polarized epithelial cell lines, such as MDCK, T84, and Caco-2, are important model systems for the study of tight junction structure and function. The Caco-2 cell line in particular is a well-established model of the intestinal epithelium (Rousset 1986), and the study of tight junctions using this cell line has important implications for the understanding of normal intestinal physiology as well as diseases such as inflammatory bowel disease, celiac disease, and enteric infections.

Tight junction permeability can be modified in response to physiological and pathophysiological stimuli, and one important regulator of permeability is myosin light chain kinase (MLCK). Although the molecular mechanisms are incompletely defined, it is clear that increased MLCK activity can increase tight junction permeability in epithelia and endothelia. This mechanism appears to have direct relevance to physiological tight junction regulation as well as dysfunction in a variety of infectious and inflammatory diseases (Clayburgh et al. 2004b).

The recent development of siRNA technology to reduce expression of specific target genes has provided a new method of probing tight junction regulatory pathways in cell models. Unfortunately, the Caco-2 cell line is relatively resistant to transfection, making the use of siRNA technology technically difficult. In particular, Caco-2 cells must be transfected in suspension before plating, after which the cells typically require a week or more of culture to develop functional tight junctions. Given that most siRNAs have a half-life within cells of less than 4 days, traditional methods of Caco-2 transfection are not adequate for siRNA-mediated knockdown.

We used siLentFect lipid reagent to provide efficient siRNA transfection of Caco-2 cells. Knockdown using siLentFect-mediated transfection of siRNA and high-density plating of Caco-2 cells allowed the early development of tight junctions, permitting the study of tight junction physiology. With this method, we were able to interfere with expression of MLCK1, a splice variant of MLCK, and to study the effect on electrophysiology.

Methods

Tissue Culture

Cells from the BBe clone of the Caco-2 cell line (Peterson and Mooseker 1992) expressing the intestinal Na^+-glucose cotransporter SGLT1 (Turner et al. 1996) were plated on Transwell permeable supports (Corning Inc., Corning, NY, USA) as described previously (Turner et al. 1997).

siRNA Design and Transfection

A 207 bp sequence (nucleotides 1,428–1,634) unique to the MLCK1 splice variant was used to design the MLCK1 *SMART*pool siRNA (Dharmacon, Lafayette, CO, USA). For transfection, 10 µl of 50 µM MLCK1 *SMART*pool siRNA or 25 µl of a 20 µM nonspecific control siRNA mix was added to 500 µl Opti-MEM medium (Invitrogen Corp., Carlsbad, CA, USA) and allowed to incubate for 5 min at 25°C. The siRNA solution was then added to 500 µl of Opti-MEM containing 30 µl of siLentFect lipid reagent and allowed to incubate for 30 min at 25°C to create the transfection mix. At the same time, approximately 10^7 Caco-2 BBe cells were incubated with 1.5 ml trypsin for 20 min. After trypsinization, the cells were resuspended in 5 ml of DMEM with 4.5 g glucose/L (Mediatech, Herndon, VA, USA). The cells were recovered by gentle centrifugation at 500 x g for 5 min, washed once more in DMEM followed by Opti-MEM, separated into two equal aliquots, and resuspended in 800 µl of Opti-MEM. This suspension was added to 1 ml of previously prepared transfection mix. The cell suspension and siRNA mix was then plated at high density (375,000 cells/cm^2) on Transwell permeable supports and cultured for 4 days to allow tight junction assembly and polarization before use in electrophysiology experiments.

Analysis of Transfected Monolayers

To isolate RNA for RT-PCR, monolayers were scraped into TRIzol reagent (Invitrogen), and RNA was extracted with chloroform, precipitated with isopropanyl alcohol, and resuspended in DEPC-treated water. Quantitation of MLCK1 and MLCK2 mRNA levels was performed using primers TCTGAGAAGAACGGCATG and ACTTCAGGGGGTGGATTC. All reactions were cycled 36 times using an iCycler® thermal cycler, with an annealing temperature of 57°C. The PCR products were separated on a 1% agarose gel and

visualized using ethidium bromide. The band intensity was measured using ImageQuant software (Amersham Biosciences, Piscataway, NJ, USA), and the MLCK1 content was calculated as (MLCK1 intensity)/(MLCK1 + MLCK2 intensity). See Clayburgh et al. (2004a) for more details.

Cell monolayers were lysed, and the lysate was separated by SDS-PAGE and immunoblotted using MLCK1-specific antisera. The band corresponding to MLCK1 was detected with horseradish peroxidase-conjugated secondary antisera (Cell Signaling Technology, Inc., Beverly, MA, USA), and the blot was visualized by enhanced chemiluminescence.

Electrophysiological measurements were made with agar bridges and Ag/AgCl calomel electrodes, as previously described (Turner et al. 1997). Briefly, monolayers were transferred from culture medium to Hank's balanced salt solution (HBSS) with 15 mM HEPES (pH 7.4) and 25 mM glucose to activate Na^+-glucose cotransport. Electrical potential differences were measured before and after application of a 50 µA current, and transepithelial resistance (TER) was determined using Ohm's law.

Results and Discussion

To determine the effectiveness of siRNA-mediated knockdown of MLCK1 in transfected Caco-2 cells, we performed semiquantitative RT-PCR of RNA from cells transfected with either nonspecific control siRNA or MLCK1-specific siRNA (Figure 1A). We observed a significant decrease in MLCK1 mRNA in cells transfected with MLCK1-specific siRNA. MLCK1 mRNA content of monolayers transfected with control siRNA was 52 ± 3% of the total MLCK expressed. MLCK1 mRNA was reduced to 27 ± 2% of total MLCK mRNA, a 47 ± 4% reduction, in monolayers transfected with MLCK1-specific siRNA. MLCK2 mRNA content was unchanged by the MLCK1-specific siRNA.

We confirmed that siRNA reduced expression of MLCK1 by immunoblotting cell lysates with MLCK1-specific antisera (Figure 1B). Cells transfected with the specific siRNA, but not the control siRNA, showed a significant reduction in the amount of MLCK1 protein. This reduction in MLCK1 expression had a significant effect on the tight junction permeability of the Caco-2 monolayers: Monolayers of cells transfected with MLCK1 siRNA exhibited a significant increase in transepithelial resistance compared to those transfected with nonspecific siRNA (Figure 2). Since MLCK activity is known to decrease TER (Turner et al. 1997), this result suggests that MLCK1 makes an important contribution to tight junction regulation in Caco-2 cells.

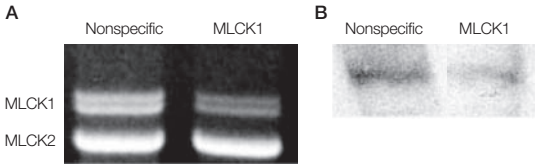

Fig. 1. Knockdown of MLCK1 in transfected Caco-2 cells.* **A**, RT-PCR of MLCK splice variants MLCK1 (upper band) and MLCK2 (lower band) from Caco-2 monolayers transfected with nonspecific or MLCK1-specific siRNA. **B**, immunoblots of lysates from monolayers transfected with nonspecific and MLCK1-specific siRNA with MLCK1-specific antisera. A significant drop in MLCK1 mRNA and protein expression is observed in monolayers transfected with MLCK1-specific siRNA.

Conclusions

In this study, we successfully knocked down the expression of a single splice variant of MLCK in Caco-2 cells using siLentFect lipid reagent to transfect siRNA. The use of siLentFect in conjunction with high-density plating allowed us to measure the effects of siRNA transfection on tight junction physiology. This method permits the use of siRNA technology in the study of Caco-2 cell physiology and barrier function and can contribute to generating further insight into molecular regulation of intestinal permeability.

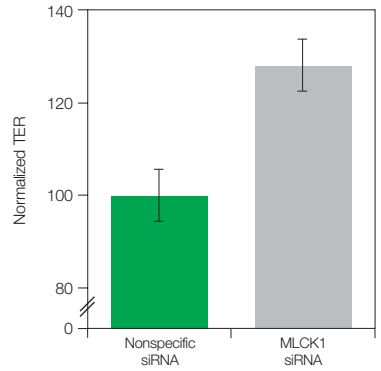

Fig. 2. Normalized TER in Caco-2 monolayers transfected with nonspecific and MLCK1-specific siRNA.* TER was normalized to monolayers transfected with nonspecific siRNA. TER was significantly higher in monolayers transfected with MLCK1-specific siRNA. Error bars represent standard error.

* Data from Clayburgh et al. (2004a).

References

Clayburgh DR et al., A differentiation-dependent splice variant of myosin light chain kinase, MLCK1, regulates epithelial tight junction permeability, J Biol Chem 279, 55506–55513 (2004a)

Clayburgh DR et al., A porous defense: the leaky epithelial barrier in intestinal disease, Lab Invest 84, 282–291 (2004b)

Peterson MD and Mooseker MS, Characterization of the enterocyte-like brush border cytoskeleton of the C2BBe clones of the human intestinal cell line, Caco-2, J Cell Sci 102, 581–600 (1992)

Rousset M, The human colon carcinoma cell lines HT-29 and Caco-2: two in vitro models for the study of intestinal differentiation, Biochimie 68, 1035–1040 (1986)

Turner JR et al., Carboxy-terminal vesicular stomatitis virus G protein-tagged intestinal Na^+-dependent glucose cotransporter (SGLT1): maintenance of surface expression and global transport function with selective perturbation of transport kinetics and polarized expression, J Biol Chem 271, 7738–7744 (1996)

Turner JR et al., Physiological regulation of epithelial tight junctions is associated with myosin light-chain phosphorylation, Am J Physiol 273, C1378–1385 (1997)

The data presented here were previously published as Figures 7A, C, and D and associated methods in the Journal of Biological Chemistry 279, 55506–55513 (2004a) and are reprinted with permission from the American Society for Biochemistry and Molecular Biology.

For additional copies of this article, request bulletin 5370.

Fractionation by Liquid-Phase Isoelectric Focusing in the MicroRotofor™ Cell: Improved Detection of Low-Abundance Proteins

Adriana Harbers, Gabriela Rodriguez, and Tom Berkelman, Bio-Rad Laboratories, Inc., Hercules, CA 94547 USA

Introduction

The effective study of low-abundance proteins often requires a fractionation step to reduce overall sample complexity and to elevate the concentration of low-abundance proteins relative to the original sample. Formerly undetectable proteins may be enriched to levels that allow downstream analysis by 2-D gel electrophoresis/mass spectrometry (2-D/MS) and liquid chromatography/mass spectrometry (LC/MS), the two methods most commonly used in proteomics for the separation and identification of proteins. Reduction in sample complexity also minimizes signal suppression effects that may occur in MS analysis of complex samples (Wang et al. 2003).

Isoelectric focusing (IEF), an electrophoretic technique used as the first-dimension separation in a traditional 2-D gel electrophoresis workflow, is also applied as a fractionation technique upstream of both 2-D/MS (Folkesson Hansson et al. 2004, Puchades et al. 2003, Puchades and Folkesson Hansson 2005) and LC/MS (Harper et al. 2004) workflows. For 2-D/MS, sample fractionation by IEF can result in a more effective analysis by removing the proteins that are outside the pH range of the selected immobilized pH gradient (IPG) strip. This limits protein precipitation and smearing, which are often the consequences of higher protein loads, and enables the enrichment of proteins in the pI range of interest.

The MicroRotofor cell performs IEF entirely in free solution (liquid-phase IEF). Based on the Rotofor® technology used for decades for liquid-phase IEF of large sample volumes, the MicroRotofor cell was designed for efficient and reproducible IEF of samples with limited availability.

Here, the effectiveness, yield, and reproducibility of fractionation with the MicroRotofor cell were examined. Fractions were analyzed by 2-D electrophoresis using pH 3–10 IPG strips and compared to the unfractionated sample to demonstrate fractionation and protein enrichment. Selected fractions from these replicate runs were separated by 2-D electrophoresis using micro-range IPG strips. The 2-D separations were compared to equivalent separations performed on the unfractionated sample. Analysis of the gels showed improved resolution and representation of low-abundance proteins following fractionation with the MicroRotofor cell.

Methods

Protein from mouse liver tissue (1 g) was extracted using the ReadyPrep™ total protein extraction kit. Total protein concentration was determined with the *RC DC*™ protein assay, and the sample was reduced and alkylated with the ReadyPrep reduction-alkylation kit. For fractionation, the reduced and alkylated sample was diluted to a concentration of 0.6 mg/ml protein in IEF buffer (7 M urea, 2 M thiourea, 4% CHAPS, 2 mM tributylphosphine, 0.001% Bromophenol Blue, 2% w/v Bio-Lyte® 3/10 ampholytes), and a 2.7 ml sample was loaded into the focusing chamber of the MicroRotofor cell. The sample was focused at 1 W (constant) for 2.5 hr, and fractionations were performed in triplicate. The pH, volume (calculated by weight/density, 1.1 g/ml), and protein concentration were measured by the *RC DC* protein assay for each of the ten fractions collected. Prior to analysis by 2-D electrophoresis, the fractions were treated with the ReadyPrep 2-D cleanup kit and resuspended in IEF buffer, containing 0.2% (w/v) ampholytes matching the pH of the IPG strip to be used.

First-dimension separations were performed using 11 cm ReadyStrip™ IPG strips, pH 3–10 or pH 4.7–5.9, and a PROTEAN® IEF cell. Second-dimension SDS-PAGE separations were performed using 8–16% Criterion™ Tris-HCl precast gels and a Criterion Dodeca™ cell. Gels were fixed in 40% ethanol, 10% acetic acid, and stained with Flamingo™ fluorescent gel stain. Image acquisition was performed on a Molecular Imager FX™ Pro Plus system, and image analysis was performed with PDQuest™ 2-D analysis software.

Results

Reproducibility of Fractionation With the MicroRotofor Cell

The three replicate mouse liver fractionations performed in the MicroRotofor cell generated reproducible pH, volume, and protein quantity profiles, as well as reproducible recovery of sample volume and protein.

pH and protein profiles — The pH gradient generated across the ten fractions showed an average shift of only 0.15 pH units between runs, and the protein concentration of each fraction from the three fractionation runs was also reproducible (Figure 1), indicating reproducible separation and harvesting of mouse liver samples with the MicroRotofor cell.

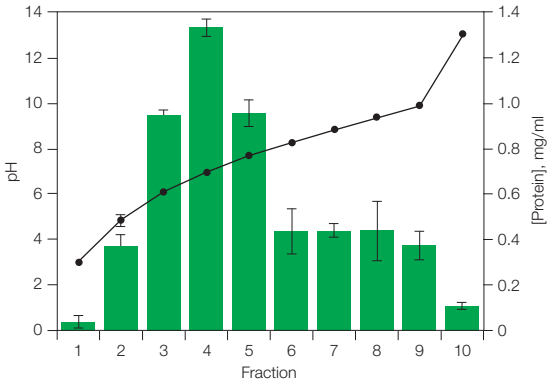

Fig. 1. Reproducibility of the pH gradient and protein distribution generated by the MicroRotofor cell. The line graph shows the mean pH values for each of the ten fractions generated after three separations of the same mouse liver sample. The bar graph shows the mean protein concentration found in each fraction after each of the three separations. Error bars indicate standard deviation.

Sample volume recovery — Regulated vacuum harvesting allowed recovery of 86–89% of the original volume loaded in the focusing chamber (Table 1). The volumes of fractions 2–9 from the three replicate runs ranged from 0.215 to 0.247 ml, differing from the run average fraction volume by ≤6% (Table 2).

Protein recovery — Protein quantitation indicated an average recovery of 77% of the initial protein amount (Table 1). Some of the protein loss may be accounted for by incomplete recovery of sample volume; no precipitate was observed in any of the fractions.

Table 1. Recovery of volume and protein. Total volume and protein recovered are shown as a percentage of the total sample loaded for separation.

	Recovery	
Run	Volume	Protein
1	89%	74%
2	89%	80%
3	86%	78%

Table 2. Reproducibility of harvesting. Volumes of fractions 2–9* were calculated from the weight of the solution divided by its density, 1.1 g/ml, and variation was calculated relative to the average fraction volume for each run. The maximum observed variation of 6% is equivalent to 14 µl. The low variability (<6%) between fractions indicates that the focusing chamber geometry and harvesting system are efficient and reliable.

	Variation in Fraction Volume		
Fraction	Run 1	Run 2	Run 3
2	–1%	–1%	–2%
3	–5%	–3%	1%
4	4%	6%	1%
5	–2%	–5%	5%
6	–3%	–4%	–3%
7	5%	4%	–1%
8	5%	5%	5%
9	–2%	–2%	–5%
Average volume	0.227 ml	0.233 ml	0.227 ml

* Fractions 1 and 10 were not used because their volumes were larger than those of fractions 2–9, due to the internal geometry of the focusing chamber.

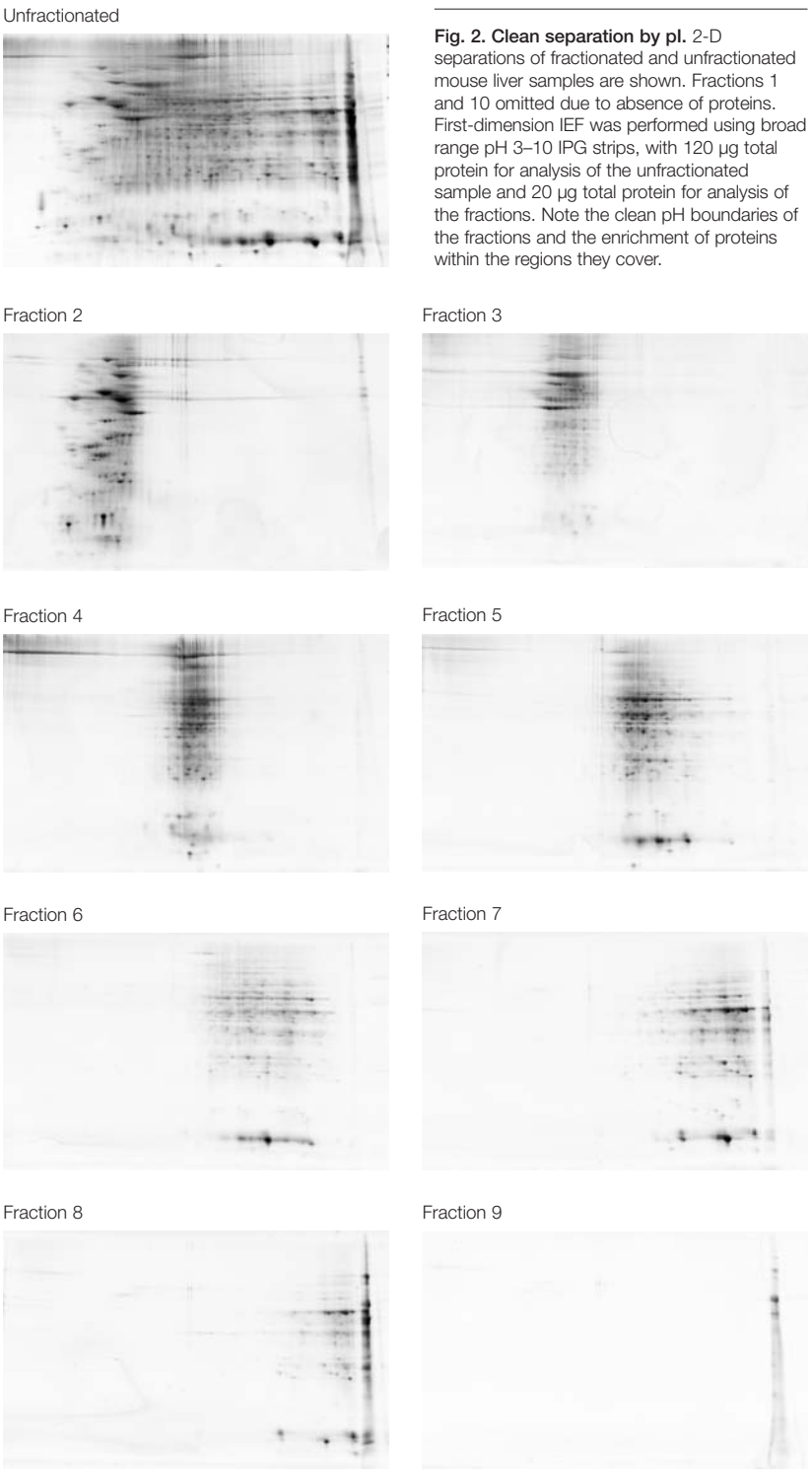

Fig. 2. Clean separation by pI. 2-D separations of fractionated and unfractionated mouse liver samples are shown. Fractions 1 and 10 omitted due to absence of proteins. First-dimension IEF was performed using broad range pH 3–10 IPG strips, with 120 µg total protein for analysis of the unfractionated sample and 20 µg total protein for analysis of the fractions. Note the clean pH boundaries of the fractions and the enrichment of proteins within the regions they cover.

Analysis of Fractionated Samples by 2-D Electrophoresis

All ten fractions from the first separation were screened using linear pH 3–10 IPG strips to demonstrate the efficacy of fractionation with the MicroRotofor cell. The 2-D gels of the ten fractions show a clearly delineated separation of the mouse liver protein sample (Figure 2).

Enrichment of Low-Abundance Proteins

To demonstrate the level of enrichment that is attainable upon fractionation with the MicroRotofor cell, a 40 µg fractionated sample was separated by 2-D electrophoresis using micro-range pH 4.7–5.9 IPG strips, and the resulting 2-D gels were compared to separations of higher protein loads (120 and 240 µg) of unfractionated sample (Figure 3). The enlarged portions of the gels in Figure 3 show that the low-abundance proteins in the 40 µg fractionated sample had identical migration patterns and much higher intensities than the same proteins in the 120 µg and 240 µg unfractionated samples. Whereas increasing the load of unfractionated sample impaired resolution without improving detection of low-abundance proteins, fractionation resulted in the clear enrichment of low-abundance proteins.

Discussion

Proteomic studies employing 2-D electrophoresis often aim to maximize the number of distinguishable individual protein species. Using narrow- or micro-range IPG strips for the first-dimension IEF separation increases the resolution of the technique; however, simply increasing the total protein load in order to bring the low-abundance proteins within the detection threshold has the undesirable side effect of incomplete and inconsistent protein intake into the IPG strip, and less effective focusing, as evidenced by smearing in the 2-D pattern (Berkelman et al. 2004).

Here, fractionation by liquid-phase IEF has been used successfully to decrease sample complexity, enhance the resolution and representation of low-abundance proteins, and improve the overall effectiveness of 2-D gel electrophoresis. Liquid-phase IEF is an effective fractionation technique: Protein loss through isoelectric precipitation is minimized by the use of highly chaotropic solutions and relatively high concentrations of carrier ampholytes, and sample proteins are not exposed to gels or other separation matrices, which can result in protein loss through adsorption.

The MicroRotofor cell simplifies liquid-phase IEF and reduces sample volume requirements. The rocking motion of the separation chamber prevents protein precipitation and settling, and the temperature control option results in reproducible separations with minimal protein modification. The carefully engineered focusing chamber and harvesting system generate reproducible fractionation with high protein recovery.

Conclusions

- Fractionations performed in the MicroRotofor cell are reproducible in terms of run-to-run fraction pH, fraction volume, and protein yield
- Fractionation with the MicroRotofor cell allows for more effective 2-D gel separations using narrow- and micro-range IPG strips by increasing the effective sample load, which minimizes the horizontal streaking seen with unfractionated sample. Fractionation preserves the overall relative abundance and position of protein spots in 2-D gels with respect to the unfractionated sample
- Protein fractionation in the MicroRotofor cell improves the 2-D resolution of low-abundance proteins that are not clearly detectable in the unfractionated sample regardless of sample load. Increased sample loads of unfractionated sample simply leads to increased streaking, which reduces resolution and obscures low-abundance proteins
- The MicroRotofor cell fulfills the requirements for an effective fractionation system and can handle samples in a volume and mass range appropriate for analysis by 2-D electrophoresis

References

Berkelman T et al., Tips to prevent streaking on 2-D gels, Bio-Rad bulletin 3110 (2004)

Folkesson Hansson S et al., Validation of a prefractionation method followed by two-dimensional electrophoresis — applied to cerebrospinal fluid proteins from frontotemporal dementia patients, Proteome Sci 2, 7 (2004)

Harper RG et al., Low-molecular-weight human serum proteome using ultrafiltration, isoelectric focusing, and mass spectrometry, Electrophoresis 25, 1299–1306 (2004)

Puchades M et al., Proteomic studies of potential cerebrospinal fluid protein markers for Alzheimer's disease, Brain Res Mol Brain Res 118, 140–146 (2003)

Puchades M and Folkesson Hansson S, The Rotofor system as a prefractionation device used prior to 2-D gel electrophoresis, Bio-Rad bulletin 3131 (2005)

Wang MZ et al., Analysis of human serum proteins by liquid phase isoelectric focusing and matrix-assisted laser desorption/ionization-mass spectrometry, Proteomics 3, 1661–1666 (2003)

For an expanded version of this article, request bulletin 5344.

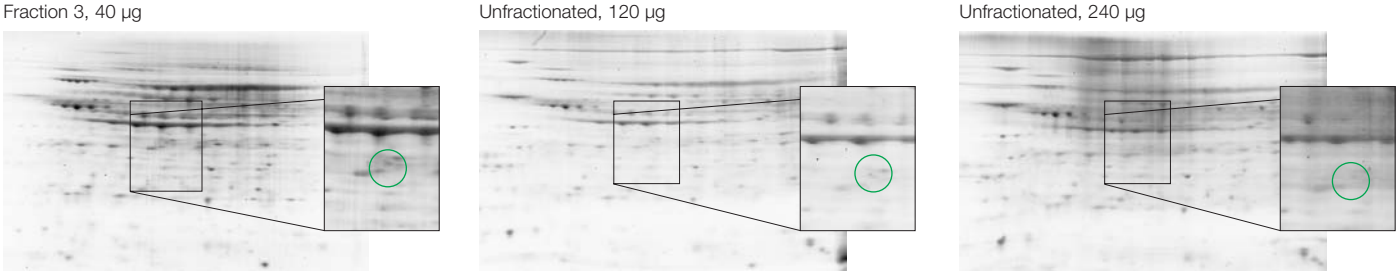

Fig. 3. Resolution of low-abundance proteins following fractionation in a MicroRotofor cell. 2-D separations of fractionated and unfractionated mouse liver samples are shown. First-dimension IEF was performed using micro-range pH 4.7–5.9 IPG strips to demonstrate the level of enrichment attainable upon fractionation with the MicroRotofor cell.

Genotyping by Arrayed Primer Extension (APEX) Using the BioOdyssey™ Calligrapher™ MiniArrayer

Alyson WM Wong,[1] Jian Ruan,[1] Ben W Tripp,[1] Luis Ugozzoli,[2] and Scott J Tebbutt,[1]
[1]James Hogg iCAPTURE Centre for Cardiovascular and Pulmonary Research, St. Paul's Hospital, University of British Columbia, Vancouver, BC, V6Z 1Y6, Canada, and [2]Bio-Rad Laboratories, Inc., Hercules, CA 94549 USA

Introduction

With the completion of the Human Genome Project, the use of molecular technologies for the study of human genetic variation has increased considerably. The identification and study of single nucleotide polymorphisms (SNPs) promise to increase our understanding of how genetic factors contribute to disease. Genotyping based on SNPs is increasingly used in both human genetic studies, and in pharmacogenomics to elucidate the genetic basis of differing responses to therapeutics.

For SNP detection, laboratories need specific, reliable, high-throughput methods that can be easily automated. One strategy to reduce cost and increase throughput is SNP detection using DNA microarrays. Microarray-based genotyping allows simultaneous testing of multiple SNPs from a single human DNA sample (Wang et al. 1998). In our laboratory, we use a genotyping method that combines DNA microarrays with APEX technology (Syvanen et al. 1990, Ugozzoli et al. 1992, Kurg et al. 2000, Tebbutt et al. 2004).

APEX is a genotyping method involving hybridization of sample DNA to specific oligonucleotide primers followed by single-nucleotide extension. The first step requires amplification of target DNA sequences containing SNP(s) using PCR. Subsequently, fragmented PCR products are hybridized to SNP-specific primers immobilized on the microarray slide via their 5' ends. The oligonucleotides are designed to be complementary to the SNP loci of interest, with the final 3' nucleotide immediately adjacent to the polymorphic base. After primer hybridization, the SNP-specific extension reaction is performed using differentially labeled fluorescent dideoxynucleotide triphosphate (ddNTP) terminators and a thermostable DNA polymerase. Finally, microarray slides are scanned, and the spot intensity data obtained using softWoRx microarray image analysis software (Applied Precision, LLC) are used for genotype analysis by SNP Chart software (Tebbutt et al. 2005).

Methods

Seven SNP loci (rs1382938, rs1417269, rs1451613, rs1467372, rs1484729, rs1506508, and rs1932819) from three human DNA samples obtained from the National Institute of General Medical Sciences (NIGMS) Human Genetic Cell Repository at the Coriell Institute for Medical Research (**http://coriell.umdnj.edu/**) and one negative control were amplified using PCR with dUTP and dTTP at a 1:4 ratio using HotStarTaq DNA polymerase (QIAGEN). PCR products were then precipitated and fragmented using uracil N-glycosylase, and fragmented DNA and untreated sample were analyzed by electrophoresis on agarose gels.

APEX and allele-specific APEX oligonucleotide primers for the detection of the seven SNP loci, as well as control APEX primers, were printed onto CodeLink slides (Amersham Biosciences) using the BioOdyssey Calligrapher miniarrayer. Primers were at 50 pmol/µl in 150 mM sodium phosphate print buffer (pH 8.5) and were printed to specific grid positions on the microarray slides according to the manufacturer's recommended protocols. The 5' end of each oligonucleotide probe was amino-modified, allowing its covalent attachment to the slide. Array quality was checked by staining with fluorescent SYBR Green II.

APEX reactions were performed on the arrayed slides as described previously (Tebbutt et al. 2004), and the slides were subsequently scanned in the arrayWoRx biochip reader (Applied Precision, LLC). Array experiments were performed in triplicate for each sample. Gridding and segmentation analysis were performed on four individual gray-scale TIFF images to create the false-color blended images shown in Figure 1. Spot intensity data for each of the four fluorescent channels (A, C, G, T) were imported into SNP Chart software, where genotype calling was performed (Tebbutt et al. 2005).

A. Sample 1

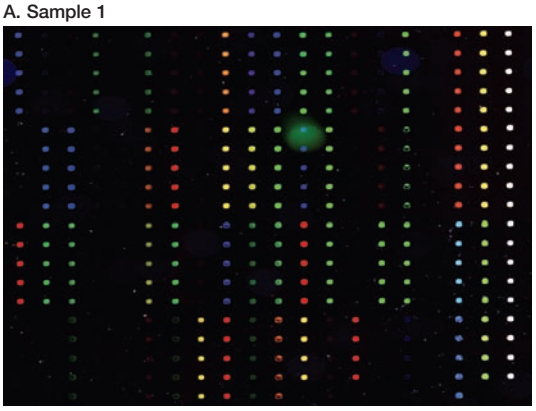

B. Sample 2

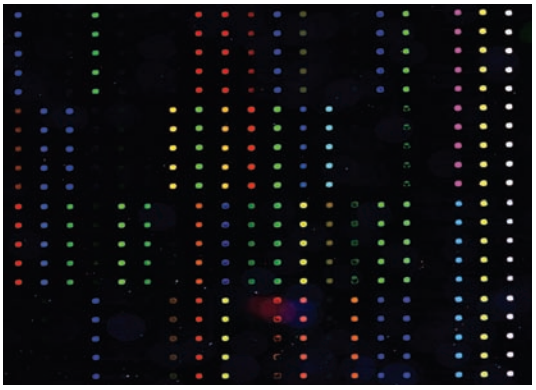

C. Sample 3

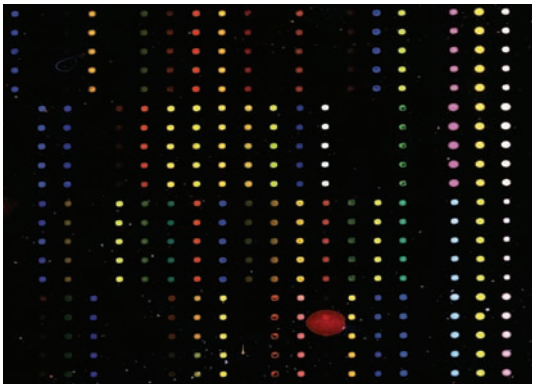

D. Negative PCR control sample

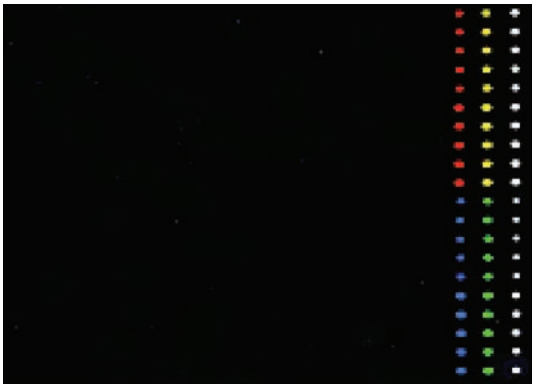

Fig. 1. False-color images of selected arrays from APEX genotyping results of Coriell samples. A–C, samples 1, 2, and 3, respectively. Colored spots indicate APEX or allele-specific primers that have been extended by a single base, with color specificity indicating which base has been incorporated. The final 3 columns in each panel show positive-control APEX probes. • = A; • = C; • = G; • = T. **D**, false-color image of a negative PCR control from APEX; only positive controls generated a signal.

Results and Discussion

The genotyping results obtained for the three samples were compared to previously validated genotypes. Of the total 21 possible genotypes (7 SNPs for each of 3 Coriell samples), all 21 were called correctly, an overall accuracy of 100%.

Figure 1 shows blended false-color images of selected arrays for each of the three human DNA samples obtained from Coriell (Figure 1A–C) and a negative control (Figure 1D).

Conclusions

This study demonstrates the successful use of the BioOdyssey Calligrapher miniarrayer for microarray-based genotyping by APEX. The arrayed primers are precisely placed by the miniarrayer, allowing easy downstream data analysis.

References

Kurg A et al., Arrayed primer extension: solid-phase four-color DNA resequencing and mutation detection technology, Genet Test 4, 1–7 (2000)

Syvanen AC et al., A primer-guided nucleotide incorporation assay in the genotyping of apolipoprotein E, Genomics 8, 684–692 (1990)

Tebbutt SJ et al., Microarray genotyping resource to determine population stratification in genetic association studies of complex disease, Biotechniques 37, 977–985 (2004)

Tebbutt SJ et al., SNP Chart: an integrated platform for visualization and interpretation of microarray genotyping data, Bioinformatics 21, 124–127 (2005)

Ugozzoli L et al., Detection of specific alleles by using allele-specific primer extension followed by capture on solid support, Genet Anal Tech Appl 9, 107–112 (1992)

Wang DG et al., Large-scale identification, mapping, and genotyping of single-nucleotide polymorphisms in the human genome, Science 280, 1077–1082 (1998)

Multiplex qPCR With iQ™ Multiplex Powermix

iQ multiplex powermix is a robust mix that greatly simplifies real-time detection of multiple targets in a single tube. With this reliable mix, you can increase throughput and control costs by running multiple assays in a single reaction, maximizing the amount of data collected from limited amounts of sample. iQ multiplex powermix is formulated for analysis using cDNA, genomic DNA, and plasmids, and can be used for a wide variety of applications, including gene expression analysis, SNP genotyping and SNP analysis, GMO detection, and viral load detection. This preblended mix provides:

- Reliable real-time multiplex detection of up to 5 unique targets, one of which may differ 10^6-fold in expression
- Linearity over 6 orders of magnitude of input cDNA and 4 orders of magnitude of input genomic DNA
- A convenient, ready-to-use format suitable for use on a wide spectrum of real-time thermal cyclers

Although design software has made it easier to design effective primers and probes, finding a set of reaction conditions that amplifies all targets with equal efficiency in both singleplex and multiplex reactions can still be a challenge. Careful primer and probe design can help mitigate the need for optimization of multiplex reactions.

Several steps are taken when designing primers and probes for multiplex qPCR. First, individual sets of primers and probes for each target are designed, taking into consideration that there should be no cross-hybridization between any of these sets. Next, the primers are optimized in singleplex SYBR Green I-based qPCR assays to ensure that the primer set in question delivers a high-quality product, without the formation of any primer-dimers or other PCR artifacts. Melt-curve and agarose gel analysis can be used to determine the quality of the PCR product. At this point, primers can be redesigned if results yield any artifacts. Once it has been established that the primer pairs yield an efficient and specific reaction, the corresponding probes can be validated. Inclusion of real-time PCR probes should not alter the efficiency of the reaction. Next, the individual reactions are ready to be combined to validate whether the multiplex reaction will perform without compromising the singleplex reaction efficiencies.

Figure 1 shows that efficient primer and probe design enables robust amplification under both singleplex and multiplex conditions, in both four- and five-target amplification schemes. Careful primer and probe design also allows accurate detection of a low-expression target in a background of three or four high-expression targets, where the range in target gene expression can be as broad as 10^6-fold.

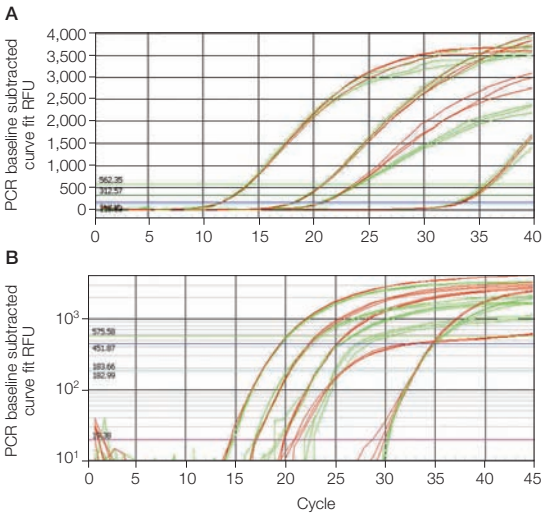

Fig. 1. Successful four- or five-target detection using iQ multiplex powermix on the iQ™5 real-time detection system. **A**, four cDNA targets were amplified using iQ multiplex powermix. Whether amplified in singleplex (red) reactions or as a four-target multiplex (green), the C_T values remained the same. Amplicons from left to right are: 18S rRNA, β-actin, α-tubulin, and IL-2. **B**, five cDNA targets were amplified using iQ multiplex powermix. Whether amplified in singleplex (red) reactions or as a five-target multiplex (green), the C_T values remained the same. Amplicons shown from left to right are: β-actin, α-tubulin, GAPDH, cyclophilin, and IL-2. Note that in both the four- and five-target detection schemes, amplification of the low expresser (IL-2) was not inhibited in the presence of three to four high-copy expressers in the multiplex reaction.

iQ multiplex powermix is a convenient option for generating multiplex qPCR results. This mix allows seamless transition between singleplex qPCR and multiplex qPCR, without compromise to threshold cycle (C_T) values or efficiency. With careful primer and probe design and testing of reactions in singleplex, this mix can readily be adopted for multiplexing protocols, minimizing the need for additional optimization of reaction or cycling conditions.

Ordering Information

Catalog #	Description
170-8848	iQ Multiplex Powermix, 50 x 50 µl reactions, 2x mix contains dNTPs (including dUTP), 11 mM $MgCl_2$, iTaq™ DNA polymerase, stabilizers
170-8849	iQ Multiplex Powermix, 200 x 50 µl reactions
170-8858	ROX Passive Reference Dye

Platform Purification of Monoclonal Antibodies With CHT™ Ceramic Hydroxyapatite

Pete Gagnon, Paul Ng, Cheryl Aberin, Julia Zhen, Jie He, Heather Mekosh, Larry Cummings, and Valerie McLaughlin,
Bio-Rad Laboratories, Inc., Hercules, CA 94547 USA

Introduction

The outstanding success and safety record of first-generation monoclonal products has triggered a surge of investment into a wide range of product applications. This has led to an immense increase in the number of product candidates that need to be evaluated, creating unprecedented pressure to develop purification processes faster.

Platform purification, a concept that has emerged from the monoclonal industry, refers to a semi-generic multistep purification procedure that can be applied to a wide range of monoclonal antibodies, without extensive method scouting or optimization. The objective is to accelerate process development and get potential new products into clinical trials as rapidly as possible.

Purification Platforms

While there is a wide choice of purification platforms, nearly all employ protein A affinity chromatography for antibody capture and initial purification (Blank 2001, Shukla et al. 2002, Tressel 2004). Affinity is typically followed by an intermediate step to remove residual host cell proteins, product aggregates, leached protein A, and virus. Most platforms conclude with a polishing step, using anion exchange chromatography to remove DNA, endotoxins, and retrovirus (Curtis et al. 2003, Gottschalk 2005).

Meeting the Challenges of Monoclonal Antibody Purification

Among the major candidates for intermediate purification of monoclonal antibodies (Table 1), CHT hydroxyapatite stands out due to its unique ability to simultaneously solve two of the key challenges of monoclonal purification: removal of leached protein A, and removal of product aggregates. Their removal is essential because of possible toxicity, in the case of protein A, and increased occurrence of neutralizing antibodies, in the case of product aggregates. Protein A is affinity-complexed to the monoclonal antibody, and the complex elutes later than uncomplexed antibody. Product aggregates are difficult to remove by most purification methods.

Table 1. Candidate methods for intermediate purification of monoclonal antibodies.

	Strengths	Limitations
Anion exchange	Good removal of host cell proteins	Capacity compromised by high product pI
	Good removal of leached protein A	Seldom better than 10 mg/ml with conventional exchangers, often half that or less; compensate with higher pH (enhances deamidation), lower conductivity (may reduce pH control), higher-capacity exchangers
	Excellent removal of DNA, endotoxin, and retrovirus, even in flow-through mode	Irreversible binding of DNA on all "Q" media
	IgG fully soluble under loading conditions	
Cation exchange	Very good removal of host cell proteins	Most IgGs partially insoluble under conditions required to support good binding capacity; compensate with online dilution
	Very good removal of leached protein A	Antibodies form stable ionic complexes with DNA, endotoxin, and other contaminants, and carry them through the method; compensate by raising pH and conductivity on high-capacity exchangers. This reduces capacity but gives better performance and reproducibility
	Fair to good removal of DNA and endotoxin	Corrosive buffers
	Good capacity, even on conventional exchangers	
	3–5x more capacity on high capacity exchangers (40–60 mg/ml)	
Hydroxyapatite	Good to very good removal of host cell proteins	Media unstable below pH 6.25 in citrate or EDTA
	Good to very good removal of leached protein A	Non-phosphate buffers cause slow degradation
	Good to very good removal of DNA and endotoxin	Medium scavenges metal contaminants that displace calcium and cause discoloration
	Very good to excellent removal of aggregates	Ceramic composition requires special care during packing and unpacking
	Excellent removal of metal contaminants (improves product homogeneity and product stability)	
	IgG fully soluble under loading conditions	
Hydrophobic interaction	Good removal of host cell proteins	Compromise: Stronger ligands give better capacity and do so at lower salt concentration, but with lower recovery and higher risk of creating aggregates
	Fair removal of leached protein A	Weaker ligands require very high salt concentrations to achieve good capacity. They give good recovery, and little or no aggregation, but elute in high salt and require online dilution to load the sample
	Fair to good removal of aggregates	Concentrated salts are corrosive or "encrustive"
	Excellent removal of DNA and endotoxin	Ammonium and phosphates pose disposal challenges
		Citrate is viscous; sodium sulfate has limited solubility

How CHT Works

Hydroxyapatite is a mineral of calcium phosphate ($Ca_{10}(PO_4)_6OH_2$). Nanocrystals are formed under special reaction conditions, agglomerated into particles, then sintered at high temperature to form a robust ceramic form of hydroxyapatite. The calcium and phosphate residues interact with proteins and other biomolecules by different mechanisms, allowing CHT to serve as a "mixed-mode resin" (Gagnon 1996, Gorbunoff 1984). The interaction with CHT phosphate groups is simple cation exchange: Positively charged amino groups form ionic bonds with negatively charged CHT phosphates. These interactions can be suspended, as with any cation exchanger, by neutral salts like NaCl, or by buffering salts such as phosphate. Carboxyl clusters on proteins form metal affinity bonds with CHT calcium. These interactions are much stronger than ionic interactions, and cannot be suspended at any concentration of NaCl. On the other hand, phosphate buffer has a higher affinity for CHT calcium than proteins have, and is thus effective for elution.

Two types of CHT are available: Type I is sintered at 400°C, while Type II is sintered at 700°C. This produces differences in pore size distribution and surface area (Table 2). Type I generally has the highest capacity for IgG antibodies, ranging from 25 mg/ml to in excess of 60 mg/ml on 40 µm media at 300 cm/hr. The 20 µm media offer higher capacity and sharper resolution, but are unsuitable for industrial columns with frit porosities ≥20 µm. They also generate higher backpressure under flow. The 80 µm media support excellent flow properties but have lower capacity than the 40 µm, leaving 40 µm as the best choice for large-scale process applications.

Traditional methods for CHT chromatography have used phosphate gradients to simultaneously disrupt metal affinity and cation exchange interactions. While this allows some removal of aggregates and leached protein A, the quality of separation is limited and variable. Achieving consistent high-quality separations requires that the metal affinity and cation exchange interactions be controlled individually. This can be done by maintaining a constant level of phosphate (5, 10, or 15 mM) throughout the column equilibration, sample load, wash, and elution steps. The low level of phosphate weakens metal affinity interaction but leaves the cation exchange interaction largely intact; most antibodies can then be eluted in a gradient up to 2 M NaCl.

Removal of leached protein A and aggregate is generally most effective at the lowest phosphate concentration (Table 3, Figure 1). Commence at 5 mM phosphate, and go higher only if necessary.

Another advantage of this elution strategy is that it simultaneously maximizes endotoxin and DNA removal (Gagnon 2005). Both DNA and endotoxin are heavily phosphorylated, resulting in a high affinity for CHT calcium, which requires a correspondingly high concentration of phosphate for elution; for example, even at high concentrations of NaCl, DNA requires more than 200 mM phosphate to elute. Contrast this with IgG, which can be eluted in NaCl at 5 mM phosphate, and the separation potential becomes apparent. DNA remains bound

Table 2. Pore size distribution and surface area of CHT Types I and II.

	CHT Type I, 40 µm	CHT Type II, 40 µm
Sintering temperature	400°C	700°C
Pore diameter	600–800 Å	800–1,200 Å
Surface area	40 m^2/g	19 m^2/g
MAb capacity	25–60 mg/ml	15–35 mg/ml

Table 3. Dependence of protein A removal on phosphate concentration.

		[PO_4]		
		5 mM	10 mM	15 mM
Protein A load	in ng/ml	22	22	22
	in ng	33	33	33
Protein A pool	in ng/ml	<0.2	<0.2	<0.2
	in ng	<2.4	<1.8	<1.2
DNA load	in ng/ml	2,257	2,257	2,257
	in ng	3,386	3,386	3,386
DNA pool	in ng/ml	<1	<1	3.9
	in ng	<12	<12	23
Endotoxin load	in EU/ml	19,000	19,000	19,000
	in EU	28,500	28,500	28,500
Endotoxin pool	in EU/ml	<0.5	1	1.6
	in EU	<6	9	10

Table 4. Contaminant clearance abilities of CHT ceramic hydroxyapatite.

	Assay Results
Aggregate removal	>99% by SEC; from >40% to <1%
Leached protein A removal	90% by Cygnus test; from 55 to 5 ng/ml
DNA removal	>3 logs by PCR; down to <1 ng/ml by PicoGreen test
Endotoxin removal	7 x 10^4 by LAL test; down to 1 EU/ml

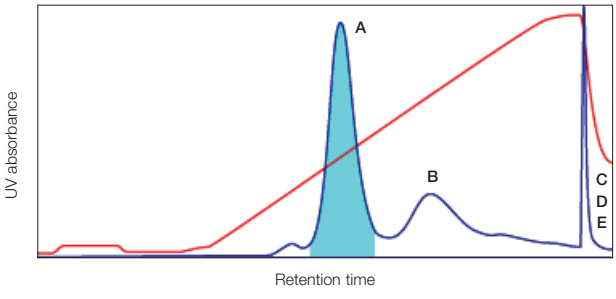

Fig. 1. Typical chromatogram for protein A-purified human IgG run on CHT. Sample was run according to the guidelines given in Table 5. **A**, native IgG; **B**, aggregates; **C**, **D**, **E**, leached protein A, DNA, endotoxin; red trace, NaCl gradient.

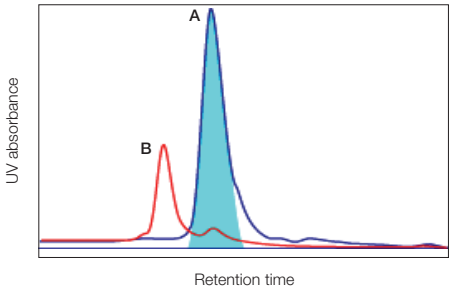

Fig. 2. Demonstration that IgG purified on CHT is free of aggregates. Results (overlaid) of analytical size exclusion chromatography for a native IgG pool (**A**) and aggregate pool (**B**) on a Bio-Sil® 400-5 column.

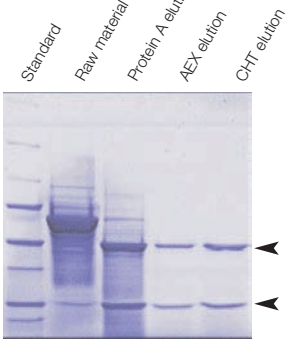

Fig. 3. Results of IgG purification using the three-step CHT platform. SDS-PAGE gel comparing sample after each step of the purification (see Table 5). Arrowheads, IgG.

throughout the NaCl gradient, and elutes only when the column is cleaned with 0.5 M phosphate. Endotoxin follows the same pattern (Figure 1). Table 4 summarizes the contaminant clearance abilities of CHT.

CHT Platform Performance

Table 5 outlines a fully integrated platform template for monoclonal purification with CHT. As indicated, the protein A elution buffer needs to be free of substances such as citric acid or EDTA that might degrade CHT. In addition, the process order is changed: If anion exchange were the terminal step, it would be necessary to perform a prior buffer exchange step to reduce the NaCl concentration of the CHT monoclonal antibody pool. Placing CHT last in the sequence avoids this compromise. Figures 2 and 3 summarize results obtained from this platform with highly aggregated human IgG_1.

Summary

This platform is easy to implement. The phosphate concentration supporting the most favorable monoclonal separation can usually be determined in two or three chromatography runs. The next step is to optimize the linear gradient slope and determine the capacity. The entire three-step process can typically be run in a half day, at a scale sufficient to supply toxicology trials. Conversion of the linear gradient to a step format, or even to a flow-through format, may be deferred until after toxicology studies, according to preference. Following such conversion, the protein A and anion exchange steps should also be optimized to ensure the best overall process performance.

Acknowledgements

Special thanks to Avid BioServices of Tustin, CA, for generously providing cell culture supernatant to support this work. Thanks also to Rolf Frey, Doug Pagano, Russ Frost, Ursula Snow, Tetsuro Ogawa, and Prof. Tsuneo Okuyama for many stimulating discussions.

References

Blank G, Design and scale-up of a MAB recovery process, presented at Recovery of Biological Products X, Cancun, Mexico (2001)

Curtis S et al., Generic/matrix evaluation of SV40 clearance by anion exchange chromatography in flow-through mode, Biotechnol Bioeng 84, 179–186 (2003)

Gagnon P, Purification tools for monoclonal antibodies, Validated Biosystems, Tucson, AZ (1996)

Gagnon P, The quest for a generic IgG purification process, presented at the Waterside Conference, Bal Harbor, FL (2005)

Gorbunoff MJ, The interaction of proteins with hydroxyapatite. I. Role of protein charge and structure, Anal Biochem 136, 425–432 (1984)

Gottschalk U, Downstream processing of monoclonal antibodies: from high dilution to high purity, Biopharm International 18, 42–58 (2005)

Shukla A et al., Generic purification processes for MAbs and Fc fusion proteins, presented at IBC conference on Scaling Up From Bench to Clinical and Beyond, San Diego, CA (2002)

Tressel T, Development of a generic platform and use of statistically designed experiments to enable rapid development of several antibodies and increase throughput for first in human antibodies, presented at IBC Conference on Antibody Production and Downstream Processing, San Diego, CA (2004)

Table 5. Three-step CHT platform for purification of monoclonal IgG.

	Protein A Medium of choice	**Anion Exchange** Flow-through mode, UNOsphere™ Q	**Hydroxyapatite** CHT Type I, 40 µm
Sample preparation	Filter to 0.22 µm	Dilute IgG pool from protein A step with 1.0 M Tris, pH 8.5, 2.8% v/v. This will yield a pH of 7.5 and conductivity of 7.5 mS/cm	Add 1% v/v 1.0 M monosodium phosphate (pH ~4.1) to the IgG pool from the previous step. This will raise the sample phosphate concentration to 5 mM and reduce the pH to 6.5
Buffers			
A	0.05 M sodium phosphate, pH 7.2	0.05 M Tris, pH 7.0–7.5	5 mM $NaPO_4$, pH 6.5
B	0.1 M glycine or arginine, 0.05 M NaCl, pH 3.8; no citrate or chelating agents	A + 1 M NaCl, pH same as buffer A	A + 1.5 M NaCl
Fractionation			
Flow	Per manufacturer's recommendation	300–600 cm/hr	300 cm/hr
Equilibrate	Buffer A	Buffer A until pH of column effluent equals buffer A	Buffer A until column effluent is pH 6.5
Load sample	20 mg IgG/ml of gel, or per manufacturer's recommendation	Volume equivalent to 100 mg IgG/ml of gel	Volume equivalent to 20 mg IgG/ml of gel
Wash	To baseline	5 column volumes (CV) buffer A	5 CV buffer A
Elute	Buffer B, to baseline	Not applicable	40 CV linear gradient to 100% buffer B
Clean	Per manufacturer's recommendation	10 CV 100% buffer B	5 CV 100% buffer C
Sanitize	Per manufacturer's recommendation	1 M NaOH	1 M NaOH
Comments	Elution pH was chosen to conform to published values for virus inactivation. NaCl in the elution buffer can improve antibody stability and solubility, which also helps to minimize aggregation. The choice between glycine and arginine may also affect aggregation and activity recovery but must be determined experimentally	In most cases, the antibody will flow through the column during sample application. If not, pH can be reduced to 7.0, or conductivity raised to 12 mS/cm, and conditions will still be within the published range shown to remove retrovirus (Curtis 2003). The Q step is sequenced ahead of the intermediate step for continuity of process flow. Otherwise, the high NaCl concentration following CHT would require an additional buffer exchange step	Native antibody will usually elute within the NaCl gradient, but if not, then increase the phosphate concentration to 10 mM. The suggested gradient is for screening. Slope and amplitude can be adjusted based on initial results. It may also be converted to a step format or run in flow-through mode. Capacity may be as high as 60 mg/ml for some monoclonals

iQ™5 Multicolor Real-Time PCR Detection System

Pass the iQ Test

What do all these images have in common? The answer is 5. Introducing the iQ5 real-time PCR detection system and reagents, bringing true five-color detection capabilities to all of your real-time PCR applications.

Five reasons why the iQ5 is the ultimate system for value and flexibility:

- **Powerful thermal gradient**
- **Optical detection system features user-changeable filter sets**
- **Gene expression analysis by relative quantity (ΔC_T) or normalized expression ($\Delta\Delta C_T$)**
- **Customizable software reports that offer comprehensive summaries of assay run conditions, data graphs and tables, and data analysis parameters**
- **Optimized multiplex reagents: increase throughput, control costs, and maximize your data output with the new iQ™ multiplex powermix**

iQ5 real-time PCR detection system and iQ multiplex powermix.

For more information, visit us on the Web at
www.bio-rad.com/products/iQ5/ or
www.bio-rad.com/supermixes/

Visit us on the Web at **discover.bio-rad.com**
Call toll free at 1-800-4BIORAD (1-800-424-6723);
outside the US, contact your local sales office.

BIO-RAD

A more favorable interaction

It's the beginning of a new era in protein discovery and function.

For more than 50 years, Bio-Rad has changed the way we look at proteins, aiding in search, discovery, and characterization. Now Bio-Rad is bringing you the ability to truly understand protein function. Whether your interest is in understanding the biological function of protein interfaces and complex formation, or in the development of antibodies and drugs for diagnostic and therapeutic applications, Bio-Rad will have a complete and total solution for you.

For more information, visit us on the Web at **www.bio-rad.com/ad/proteininteraction/**

XPR™ technology — The power of surface plasmon resonance (SPR) combined with parallel processing.

Visit us on the Web at **discover.bio-rad.com**
Call toll free at 1-800-4BIORAD (1-800-424-6723); outside the US, contact your local sales office.

BIO-RAD